ChemCatChem

Supporting Information

Meso-2-MethoxyNaphthalenyl-BODIPY as Efficient Organic Dye for Metallaphotoredox Catalysis

Elena Bassan, Francesco Calogero, Yasi Dai, Angela Dellai, Alessandro Franceschinis, Emanuele Pinosa, Fabrizia Negri, Andrea Gualandi,* Paola Ceroni,* and Pier Giorgio Cozzi*

Table of contents:

General methods and materials

Synthetic details. ^{1}H-NMR spectra were recorded on Varian Mercury 400 spectrometer. Chemical shifts are reported in ppm from TMS with the solvent resonance as the internal standard ($CHCl_3$: δ = 7.26 ppm, DMSO-d_6: δ = 2.50 ppm, CD_3CN: δ = 1.94 ppm, CD_3OD: δ = 3.31 ppm). Data are reported as follows: chemical shift, multiplicity (s = singlet, d = doublet, t = triplet, q = quartet, dd = doublet of doublets, m = multiplet), coupling constants (Hz). ^{13}C-NMR spectra were recorded on Varian Mercury 400 spectrometer. Chemical shifts are reported in ppm from TMS with the solvent as the internal standard ($CDCl_3$: δ = 77.0 ppm, DMSO-d_6: δ = 39.5 ppm, CD_3OD: δ = 49.0 ppm). Chromatographic purifications were performed with Merck 240-400 mesh silica gel. All reactions were set up under an argon atmosphere in oven-dried glassware using standard Schlenk techniques.

Anhydrous solvents were supplied by Aldrich in Sureseal® bottles. All the reagents were purchased from commercial sources (Sigma-Aldrich, Alfa Aesar, Fluorochem, Strem Chemicals, TCI) and used without further purification unless specified.

Starting Materials **2a-g** were prepared in according to the reported procedures.[1–9]

Aryl diazonium salts **3a-e** were prepared following the reported literature procedure.[10]

Reaction mixtures were irradiated with 16 W green led strip or Kessil® PR160L@525 nm (for supplier details see: https://kessil.com/products/science_PR160L.php).

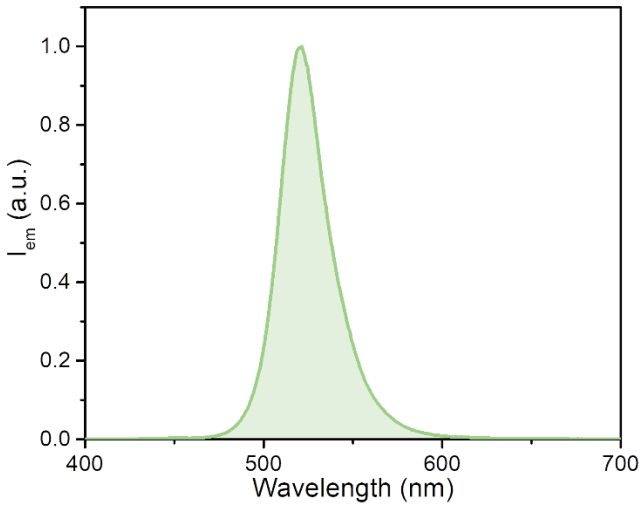

Figure S1. Emission profile of 16 W green led strip used to irradiate the solutions.

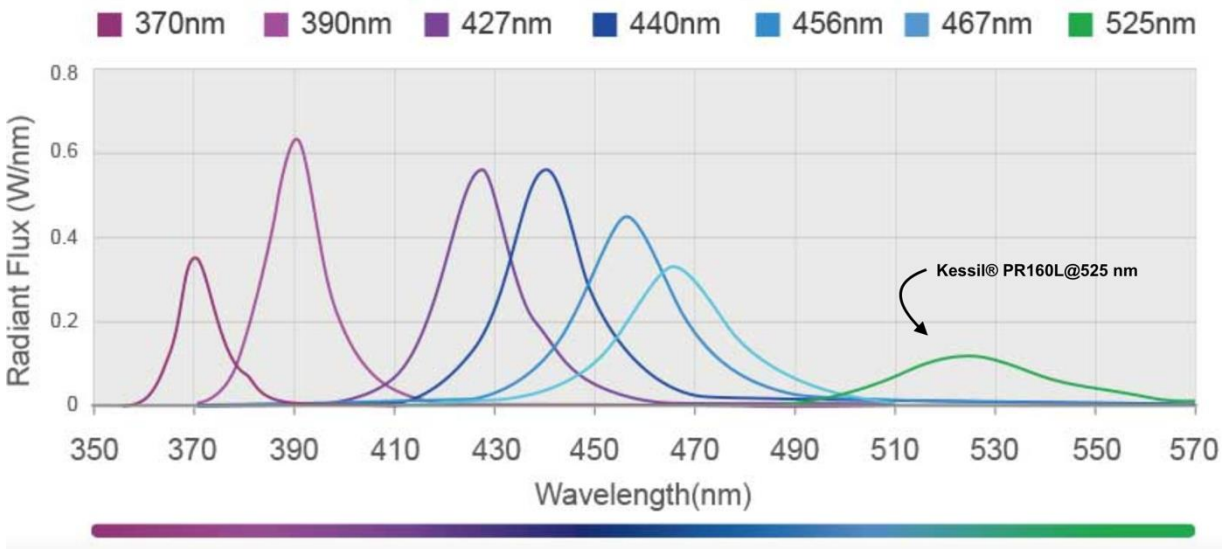

Power Consumption	370nm (max 43W), 390nm (max 52W), 427nm & 440nm (max 45W), 456nm (max 50W), 467nm (max 44W), 525nm (max 44W)
Input Voltage	100-240 VAC
Operating Temperature	0 - 40°C / 32 - 104°F
Beam Angle	56°
Wavelength Options	370nm, 390nm, 427nm, 440nm, 456nm, 467nm, 525nm
Average Intensity of PR160 series	352mW/cm2 (measured from 1 cm distance)
Dimensions (H x D)	4.49" x 2.48" / 11.4cm x 6.3cm

Figure S2. Emission profile of the Kessil® PR160L@525 nm used to irradiate the solutions.

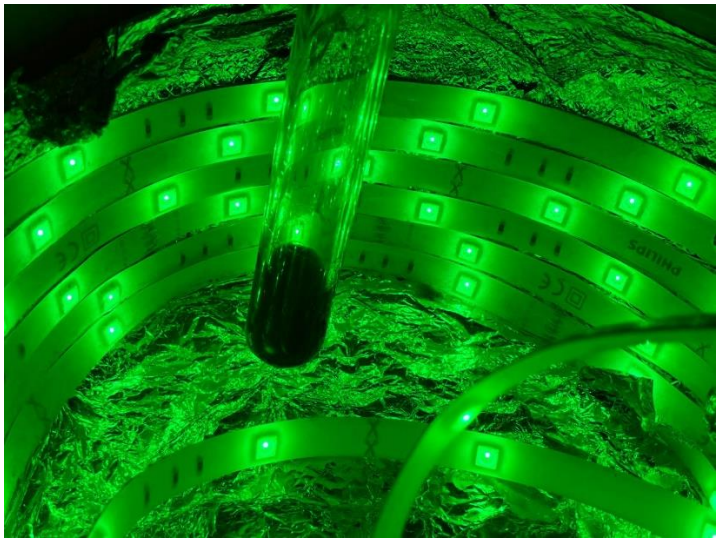

Figure S3. Standard reaction set-up with 16W green LEDs stripes. The reaction flasks were positioned approximatively at 5–10 cm from the light source. The reaction temperature was close to 25 °C during the irradiation as measured with a thermometer at 2 cm from reaction flask.

Photophysical experiments. All photophysical analyses were carried out in air-equilibrated MeOH at 298K, unless otherwise noted and degassed solutions were prepared inside a nitrogen-filled glovebox in sealed quartz cuvettes. UV-Vis absorption spectra were recorded with a PerkinElmer λ40 spectrophotometer using quartz cells with optical path length of 1.0 cm. Luminescence spectra were performed with a PerkinElmer LS-50. Fluorescence lifetimes were measured with an Edinburgh FLS920 spectrofluorometer by time-correlated single-photon counting (TCSPC) technique. Fluorescence quantum yields were measured using fluoresceine in NaOH 0.1M (Φ_{FLUO}= 95%) as the standard [11]. Singlet oxygen quantum yields were measured using Eosin Y in MeOH (Φ_{Δ}= 26%) as the standard[12] using an Edinburgh FLS920 spectrofluorometer equipped with a Ge detector. The experiments of ns-transient absorption spectroscopy were performed by an Ultrafast Systems apparatus equipped with a Hamamatsu R928 phototube connected to a Tektronix TDS3032B (400 MHz) oscilloscope and a Continuum Surelite I-10 Nd:YAG laser source (λ_{exc}: 532 nm).

Electrochemical experiments. Cyclic voltammetries were performed at room temperature by using an EcoChemie Autolab 30 potentiostat in a three-electrode setup (working electrode: glassy carbon (d = 3 mm); quasi-reference electrode: silver wire; counter electrode: Pt wire) in anhydrous MeCN (supporting electrolyte: $TEAPF_6$ 0.1 M) and using Fc^+/Fc as the internal standard (Fc^+/Fc = +0.38 V vs SCE). The working electrode was polished with 0.03 μm alumina paste, rinsed with water and acetone and finally blow-dried.

Computational details. Ground state equilibrium structure of **BDP** dyad was determined with density functional theory (DFT) calculations. The M06-2X functional was employed along with 6-311G* basis set. Solvent effects were included by means of the Polarizable Continuum Model (PCM)[13]. According to the experimental measurements, MeCN (ε=35.688) was considered as solvent. The corresponding calculation is labelled as MeCN-M06-2X/6-311G*. Excited state wavefunctions and excitation energies were calculated with time-dependent (TD)-DFT, using the same functional and basis set as indicated above. Ten triplet and ten singlet excited states were included in the calculations. Due to the constrained cyanine nature of BODIPY and the insufficient electron correlation at TD-DFT level, excitation energies are systematically overestimated by ca. 0.4-0.5 eV[14-18] at this level of theory. Nevertheless, it has been shown in several benchmark works that the M06-2X functional is suitable to describe excitation energies in BODIPY derivatives and the variations induced by side groups, modifications of the skeleton, stiffening or extension of the conjugated path [19-23] Excited state calculations are indicated as MeCN-TD-M06-2X/6-311G*. Excitation energies in solution were initially determined with the use of the standard linear response (LR). Solute-solvent polarization effects in excited states were additionally determined with the state specific (SS) corrected linear response (cLR) [24-25] approach. Only the fast solvent component was equilibrated (hereafter indicated as NEQ) in calculations of excited state energies used to model absorption spectra, while a fully equilibrated solvent was assumed (hereafter labelled EQ) for excited state energies employed to determine solvent reorganization energies and solvent-induced stabilization of excited states. Accordingly, the solvent correction included in excited state calculations is indicated by the label LR, cLR(NEQ) or cLR(EQ). All calculations were performed with the Gaussian 16 package.[26] The spin-orbit coupling (SOC) integrals were calculated with the spin-orbit mean-field (SOMF) method, with one-center approximation applied to the exchange term, (SOMF(1X)[27-28]. Relativistic corrections were included with the zeroth order regular approximation (ZORA)[29] using the ZORA-def2-TZVP basis sets. The calculations were carried out with ORCA 5.0.1 package[30] with the Tamm-Dancoff approximation (TDA).

Synthesis

Synthesis of Meso-2-Methoxynaphthalen-2-yl-BODIPY (BDP, 1)

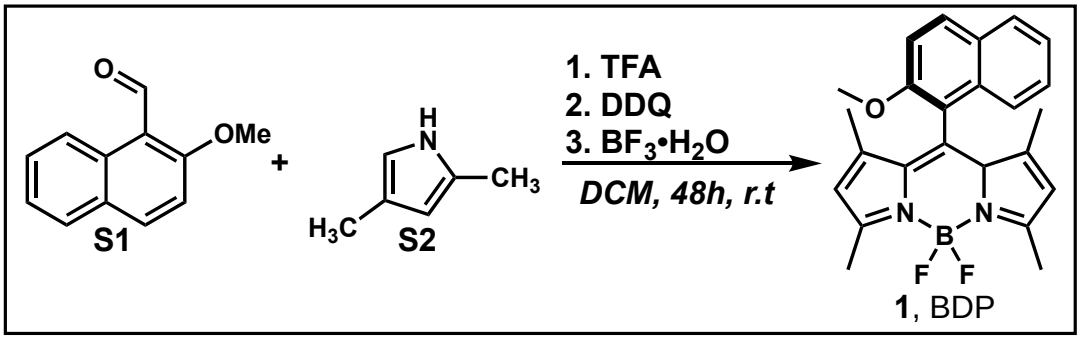

meso-2-Methoxynaphthalenyl-BODIPY (**1**) was obtained adapting the procedure described by Caruso and co-workers.[31]

Under argon atmosphere, an oven-dried 100 mL two–necked round bottom flask, equipped with a magnetic stirring bar, was charged with 2-methoxy-1-naphthaldehyde **S1** (2.24 mmol, 418 mg, 1 equiv.), freshly distilled 2,4-dimethylpyrrole **S2** (4.70 mmol, 447 mg, 484 µL, 2.1 equiv.) and dry DCM (40 mL). To this solution 6 drops of trifluoroacetic acid (TFA) were added and a color change from light green to deep red was appreciated. The reaction mixture was allowed to stir, protected from light, until ^{1}HNMR analysis of the reaction crude showed disappearance of the aldehyde **S1**.

Then, DDQ (4.4 mmol, 1.017 g, 2 equiv.) was added and the reaction was stirred for further 30 minutes and color turned from red to violet. Thereafter, triethylamine (38 mmol, 3.853 g, 5.3 mL, 17 equiv.) was added at room temperature and the resulting reaction mixture was stirred for further 30 minutes. Finally, BF_3•Et_2O (38 mmol, 5404 mg, 4.7 mL, 17 equiv.) was added and the reaction mixture was stirred overnight. The reaction mixture was subsequently washed three times with water (3 x 10 mL), the organic phase was dried over Na_2SO_4, and the solvents were removed under vacuum. The crude was purified by flash column chromatography (SiO_2, Cyclohexane/AcOEt/DCM 9:0.5:2) to afford **1** (254 mg, 28%) as a red bright solid.

TLC: Cyclohexane:DCM 60:40 *Rf* 0.16

^{1}H NMR (401 MHz, $CDCl_3$): δ 7.99 (d, *J* = 9.1 Hz, 1H), 7.84 – 7.77 (m, 1H), 7.61 (d, *J* = 1.0 Hz, 1H), 7.41 – 7.32 (m, 3H), 5.92 (s, 2H), 3.89 (s, 3H), 2.59 (s, 6H), 1.13 (s, 6H).

^{13}C{^{1}H} NMR (101 MHz, $CDCl_3$): δ 155.0, 153.4, 142.3, 137.4, 132.8, 131.0, 129.0, 127.7, 124.2, 123.8, 120.8, 117.3, 113.1, 56.4, 14.6, 13.4.
(m, $^{2}J_{FF}$ = 109.6 Hz, $^{1}J_{11BF}$ = 34.2 Hz)

^{19}F NMR (376.5 Hz, $CDCl_3$): δ -144.6 [dq (1:1:1:1 quartet), $^{2}J_{FF}$ = 109.6 Hz, $^{1}J_{11BF}$ = 34.2 Hz, 1F], -145.8 [dq (1:1:1:1 quartet), $^{2}J_{FF}$ = 109.6 Hz, $^{1}J_{11BF}$ = 31.6 Hz, 1F].

General procedure for dual photoredox and palladium-catalyzed room temperature C-H activation

All the reactions were performed in duplicate on 0.1 mmol scale of starting material **2a–h**. A dry 10 mL Schlenk tube, equipped with a Rotaflo stopcock, magnetic stirring bar and an argon supply tube, was first charged under argon with the organic photocatalyst **BDP** (**1**) (5 mol%, 0.005 mmol, 2 mg), $Pd(OAc)_2$ (10 mol%, 0.01 mmol, 2.3 mg) and the appropriate aryldiazonium salt **3a-e** (4 equiv., 0.4 mmol). Dry MeOH (3 mL in order to obtain a 0.033 M substrate solution) was then added and the reaction mixture was further subjected to a freeze-pump-thaw procedure (four cycles) and the vessel refilled with argon. The reaction was irradiated under vigorous stirring for the desired time. After that the two reaction mixtures were quenched with a saturated solution of $NaHCO_3$ (7 mL approx.), combined and extracted with AcOEt (4 x 5 mL). The combined organic layers were dried over anhydrous Na_2SO_4 and the solvent was removed under reduced pressure. The crude was subject of flash column chromatography (SiO_2) to afford the products **4** in the stated yields. The reported results were average results of two reactions.

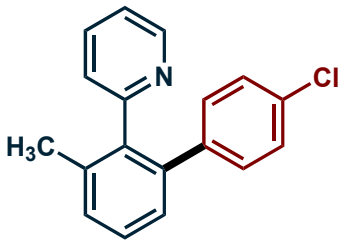

(**4a**) Clear pink viscous oil, 72% (0.144 mmol, 40 mg). The general procedure was applied using **2a** (2x 0.1 mmol, 17 mg) and **3a** (2 x 0.4 mmol, 90 mg, 4 equiv.) and performed in duplicate.

The title compound was isolated by flash column chromatography (Hexane/Et_2O 9:1).

Spectroscopic data are in agreement with those already reported in the literature. [32]

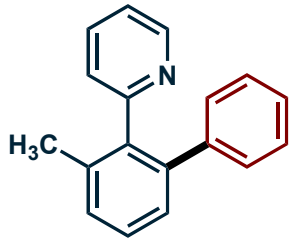

(**4b**) Clear pink viscous oil, 72% (0.144 mmol, 35 mg). The general procedure was applied using **2a** (2 x 0.1 mmol, 17 mg) and **3b** (2 x 0.4 mmol, 76 mg, 4 equiv.) and performed in duplicate.

The title compound was isolated by flash column chromatography (Hexane/AcOEt 9:1).

Spectroscopic data are in agreement with those already reported in the literature.[32]

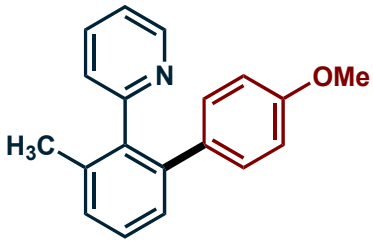

(**4c**) Clear pink viscous oil, 56% (0.112 mmol, 31 mg). The general procedure was applied using **2a** (0.2 mmol, 34 mg) and **3c** (0.8 mmol, 178 mg, 4 equiv.).

The title compound was isolated by flash column chromatography (Hexane/Et_2O 4:1).

Spectroscopic data are in agreement with those already reported in the literature.[32]

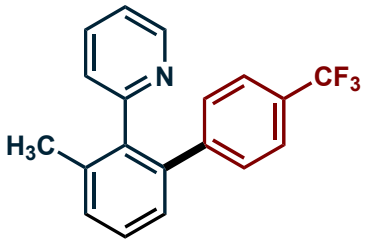

(**4d**) Clear pink viscous oil, 65% (0.130 mmol, 41 mg). The general procedure was applied using **2a** (2 x 0.1 mmol, 17 mg) and **3d** (2 x 0.4 mmol, 103 mg, 4 equiv.) and performed in duplicate.

The title compound was isolated by flash column chromatography (Hexane/Et_2O gradient from 9:1 to 85:15).

Spectroscopic data are in agreement with those already reported in the literature. [32]

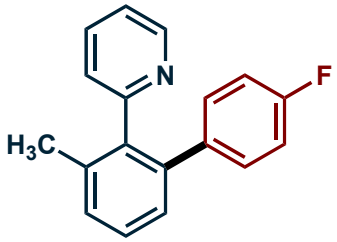

(**4e**) Clear pink viscous oil, 61% (0.122 mmol, 32 mg). The general procedure was applied using **2b** (2 x 0.1 mmol, 17 mg) and **3e** (2 x 0.4 mmol, 84 mg, 4 equiv.) and performed in duplicate.

The title compound was isolated by flash column chromatography (Cyclohexane/Et_2O 4:1).

Spectroscopic data are in agreement with those already reported in the literature. [32]

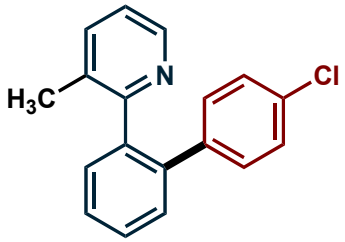

(**4f**) Clear pink viscous oil, 68% (0.136 mmol, 38 mg). The general procedure was applied using **2b** (2 x 0.1 mmol, 17 mg) and **3a** (2 x 0.4 mmol, 90 mg, 4 equiv.) and performed in duplicate.

The title compound was isolated by flash column chromatography (Hexane/Et_2O gradient from 3:1 to 1:1).

Spectroscopic data are in agreement with those already reported in the literature. [32]

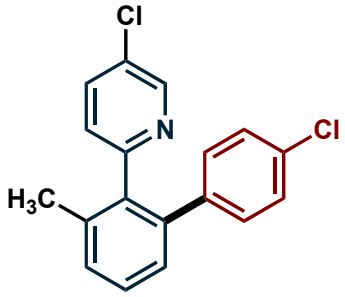

(**4g**) Clear pink viscous oil, 60% (0.120 mmol, 38 mg). The general procedure was applied using **2c** (2 x 0.1 mmol, 21 mg) and **3a** (2 x 0.4 mmol, 90 mg, 4 equiv.) and performed in duplicate.

The title compound was isolated by flash column chromatography (Hexane/Et_2O 95:5).

^{1}H NMR (401 MHz, $CDCl_3$): δ 8.58 (dd, J = 2.5, 0.8 Hz, 1H), 7.45 (dd, J = 8.3, 2.5 Hz, 1H), 7.35 (t, J = 7.6 Hz, 1H), 7.31 – 7.27 (m, 1H), 7.23 – 7.19 (m, 1H), 7.15 – 7.10 (m, 2H), 6.99 – 6.95 (m, 2H), 6.82 (dd, J = 8.3, 0.8 Hz, 1H), 2.15 (s, 3H)

^{13}C{^{1}H} NMR (101 MHz, $CDCl_3$): δ 157.4, 147.9, 140.0, 139.8, 138.0, 136.9, 135.7, 132.6, 130.8 (2C), 130.0, 129.8, 128.4, 128.0 (2C), 127.5, 126.3, 20.4.

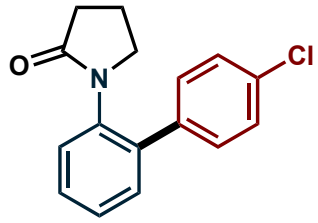

(**4h**) Clear pink viscous oil, 51% (0.102 mmol, 28 mg). The general procedure was applied using **2d** (2 x 0.1 mmol, 16 mg) and **3a** (2 x 0.4 mmol, 90 mg, 4 equiv.) and performed in duplicate.

The title compound was isolated by flash column chromatography (Cyclohexane/AcOEt 6:4).

^{1}H NMR (401 MHz, $CDCl_3$): δ 7.44 – 7.27 (m, 8H), 3.24 (t, J = 7.0 Hz, 2H), 2.41 (t, J = 8.1 Hz, 2H), 1.96 – 1.84 (m, 2H).

^{13}C{^{1}H} NMR (101 MHz, $CDCl_3$): δ 175.6, 138.5, 137.6, 136.3, 133.7, 130.7, 129.7 (2C), 128.9, 128.6 (2C), 128.4, 128.2, 50.3, 31.1, 19.0

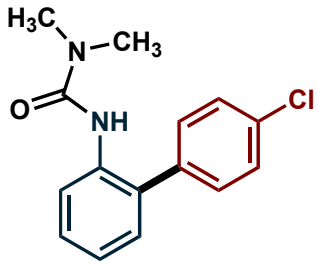

(**4i**) Clear pink viscous oil, 39% (0.08 mmol, 22 mg). The general procedure was applied using **2e** (2 x 0.1 mmol, 16 mg) and **3a** (2 x 0.4 mmol, 90 mg, 4 equiv.) and performed in duplicate.

The title compound was isolated by flash column chromatography (Cyclohexane/AcOEt 7:3).

Spectroscopic data are in agreement with those already reported in the literature.[33]

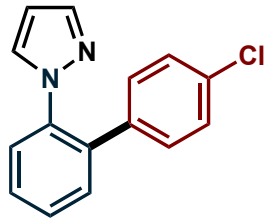

(**4j**) Clear pink viscous oil, 25% (0.050 mmol, 13 mg). The general procedure was applied using **2f** (2 x 0.1 mmol, 15 mg) and **3a** (2 x 0.4 mmol, 90 mg, 4 equiv.) and performed in duplicate.

The title compound was isolated by flash column chromatography (Cyclohexane/AcOEt 95:5).

^{1}H NMR (401 MHz, $CDCl_3$): ^{1}H NMR (401 MHz, $CDCl_3$) δ 7.61 (d, *J* = 1.8 Hz, 1H), 7.58 – 7.54 (m, 1H), 7.45–7.42(m, 3H), 7.24 – 7.22 (m, 2H), 7.09 (d, *J* = 2.4 Hz, 1H), 7.02 – 6.98 (m, 2H), 6.21 (t, *J* = 2.1 Hz, 1H).

^{13}C{^{1}H} NMR (101 MHz, $CDCl_3$): δ 140.4, 138.5, 136.9, 135.7, 133.6, 131.2, 130.8, 129.8(2H), 128.7(2H), 128.7, 128.5, 126.8, 106.7.

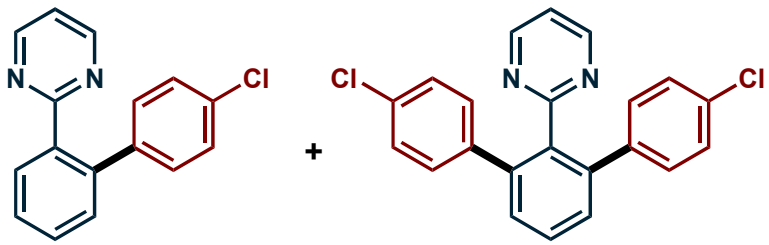

Products **4k** and **4k'** products were obtained simultaneously from the reaction mixture applying the general procedure performing the reaction in duplicate employing **2g** (2 x 0.1 mmol, 16 mg) and **3a** (2 x 0.4 mmol, 90 mg, 4 equiv.).

(**4k**) 45%, 0.09 mmol, 24 mg

The title compound was isolated by flash column chromatography (Cyclohexane/AcOEt 8:2).

^{1}H NMR (401 MHz, $CDCl_3$): δ 8.63 (d, J = 4.9 Hz, 2H), 7.82 – 7.78 (m, 1H), 7.53 – 7.44 (m, 2H), 7.41 (dd, J = 7.2, 1.8 Hz, 1H), 7.22 – 7.17 (m, 2H), 7.10 (t, J = 4.9 Hz, 1H), 7.07 – 7.02 (m, 2H).

^{13}C{^{1}H} NMR (101 MHz, $CDCl_3$): δ 167.7, 156.8 (2C), 140.2, 140.1, 138.1, 132.6, 130.6, 130.5, 130.4 (2C), 129.5, 128.1 (2C), 127.7, 118.5.

(**4k'**) 11%, 0.022 mmol, 8 mg

The title compound was isolated by flash column chromatography (Cyclohexane/AcOEt 85:15).

^{1}H NMR (401 MHz, $CDCl_3$): δ 8.47 (d, J = 4.9 Hz, 2H), 7.54 (dd, J = 8.3, 7.0 Hz, 1H), 7.44 – 7.38 (m, 2H), 7.16 – 7.09 (m, 4H), 7.07 – 7.00 (m, 4H), 6.96 (t, J = 4.9 Hz, 1H).

^{13}C{^{1}H} NMR (101 MHz, $CDCl_3$): δ 167.4, 156.2 (2C), 140.4 (2C), 139.5 (2C), 137.5, 132.8 (2C), 130.4 (4C), 129.4 (2C), 128.9, 128.1 (4C), 118.4.

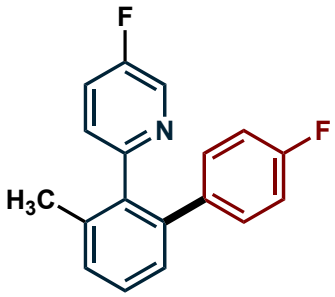

(**4l**) Clear pink viscous oil, 14% (0.03 mmol, 8 mg). The general procedure was applied using **2h** (0.2 mmol, 38 mg) and **3e** (0.8 mmol, 168 mg, 4 equiv.).

The title compound was isolated by flash column chromatography (Cyclohexane/AcOEt 4:1).

^{1}H NMR (401 MHz, $CDCl_3$): δ 8.47 (d, J = 2.9 Hz, 1H), 7.34 (t, J = 7.5 Hz, 1H), 7.27 (d, J = 7.5 Hz, 1H), 7.23 – 7.14 (m, 2H), 6.98 (ddd, J = 8.4, 5.5, 2.4 Hz, 2H), 6.88 – 6.78 (m, 3H), 2.14 (s, 3H).

^{13}C{^{1}H} NMR (101 MHz, $CDCl_3$): δ 161.6 (d, J = 245.8 Hz), 157.9 (d, J = 255.9 Hz), 155.4 (d, J = 4.4 Hz), 140.4, 138.3, 137.4 (d, J = 3.4 Hz), 137.1 (d, J = 23.3 Hz), 136.9, 131.1 (d, J = 8.0 Hz, 2C), 129.6, 128.3, 127.5, 126.4 (d, J = 4.2 Hz), 122.8 (d, J = 18.4 Hz), 114.6 (d, J = 21.3 Hz, 2C), 20.4.

^{19}F NMR (377 MHz, $CDCl_3$): δ -115.0 – -115.2 (m, 1F), -128.3 – -128.4 (m, 1F).

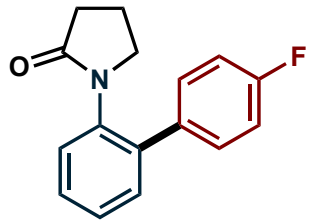

Products **4m** and **4m'** products were obtained simultaneously from the reaction mixture applying the general procedure using **2d** (0.2 mmol, 32 mg) and **3e** (0.8 mmol, 168 mg, 4 equiv.). Product **4m'** was not isolated and characterized but only observed by GC-Ms analysis of the reaction crude. **4m** was isolated by flash column chromatography (Cyclohexane/AcOEt 5:5).

(**4m**) Clear pink viscous oil, 46% (0.09 mmol, 24 mg).

^{1}H NMR (401 MHz, $CDCl_3$) δ 7.34 (dddd, J = 20.9, 17.9, 7.8, 4.8 Hz, 6H), 7.07 (t, J = 8.7 Hz, 2H), 3.22 (t, J = 7.0 Hz, 2H), 2.41 (t, J = 8.1 Hz, 2H), 1.88 (p, J = 7.5 Hz, 2H).

^{13}C{^{1}H} NMR (101 MHz, $CDCl_3$): δ 175.6, 162.4 (d, J = 246.9 Hz), 138.8, 136.4, 135.1 (d, J = 3.2 Hz), 130.8, 130.0 (d, J = 8.0 Hz, 2C), 128.7, 128.4, 128.1, 115.4 (d, J = 21.4 Hz, 2C), 50.2, 31.1, 19.0.

^{19}F NMR (377 MHz, $CDCl_3$): δ -113.4 – -113.6 (m, 1F).

Photophysical studies

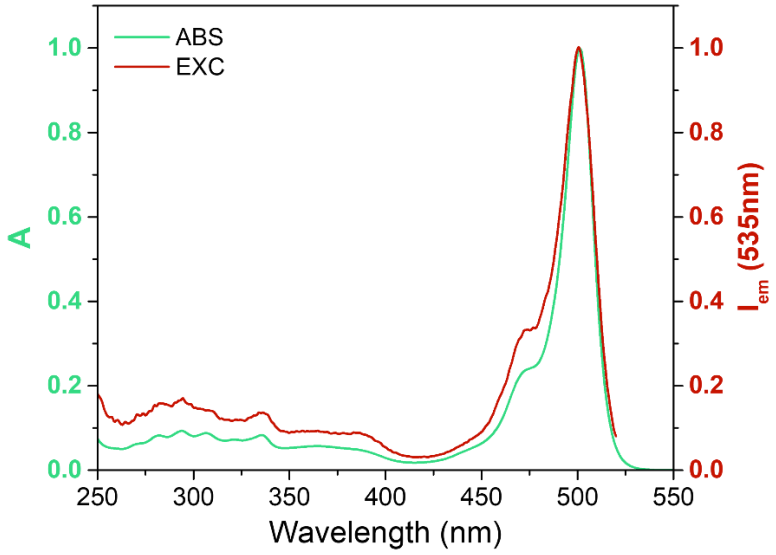

Figure S4. Normalized absorption spectra (green line) and excitation spectra (red line, λ_{em}: 535nm) of **BDP** in MeCN.

The excitation spectrum recorded for **BDP** matches the absorption spectrum of the dyad and displays the peaks corresponding to the BODIPY core (525-450 nm) and the peaks corresponding to the 2-methoxynaphtalenyl unit (250-350 nm). This result proves that, in the dyad, energy transfer between the two constituting units is occurring with unitary efficiency.

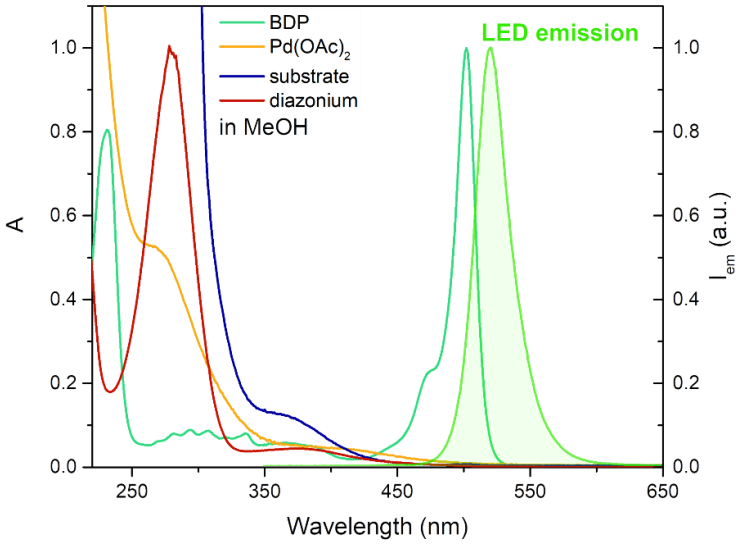

Figure S5. Normalized absorption spectra of **BDP**, $Pd(OAc)_2$, substrate and diazonium salt in MeOH and emission spectra of the green LED used for irradiation.

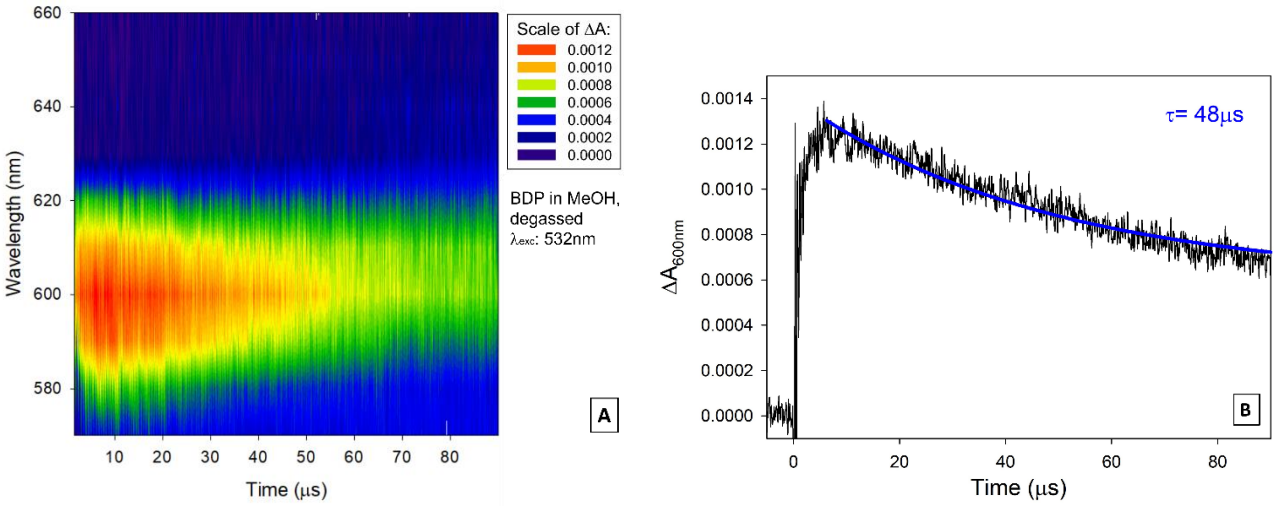

Figure S6. A) Transient absorption spectrum of **BDP** in degassed MeOH, λ_{exc}: 532nm. **B)** Corresponding decay profile at 600nm.

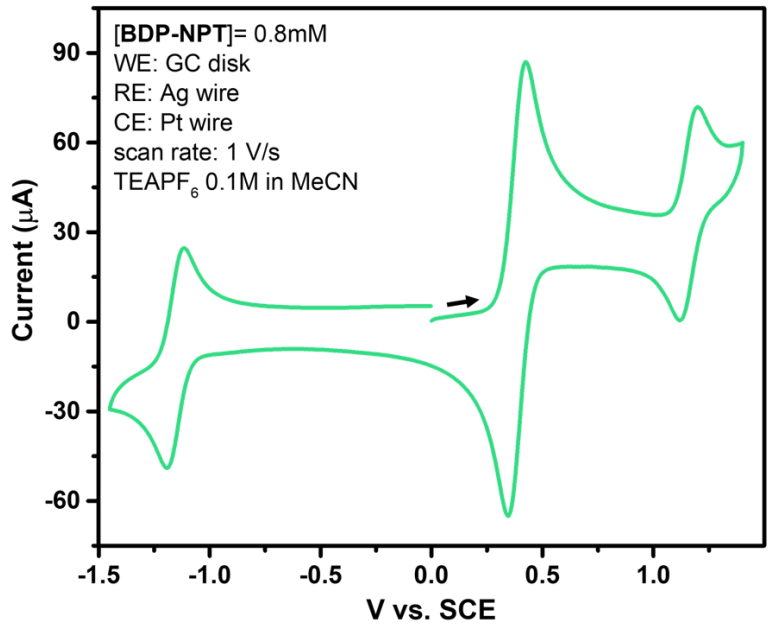

Figure S7. Cyclic voltammetry of **BDP** 0.8mM in degassed MeCN. WE: glassy carbon disk; quasi-RE: Ag wire; CE: Pt wire, scan rate: 1 V/s; supporting electrolyte: $TEAPF_6$ 0.1M; internal standard: ferrocene (+0.39 V vs. SCE).

Cyclic voltammetry of **BDP** 0.8mM in degassed MeCN. WE: glassy carbon disk; quasi-RE: Ag wire; CE: Pt wire, scan rate: 1 V/s; supporting electrolyte: $TEAPF_6$ 0.1M; internal standard: ferrocene. Ferrocene's peak has been grayed out for clarity.

Table S1. Photophysical characterization of **BDP** in MeOH.

	ε ($M^{-1}cm^{-1}$)	λ_{MAX}^{ABS} (nm)	λ_{MAX}^{FLUO} (nm)	ϕ_{FLUO}	τ_{S_1} (ns)	ϕ_{Δ}
BDP	59000	502	513	76%	6.9	14%

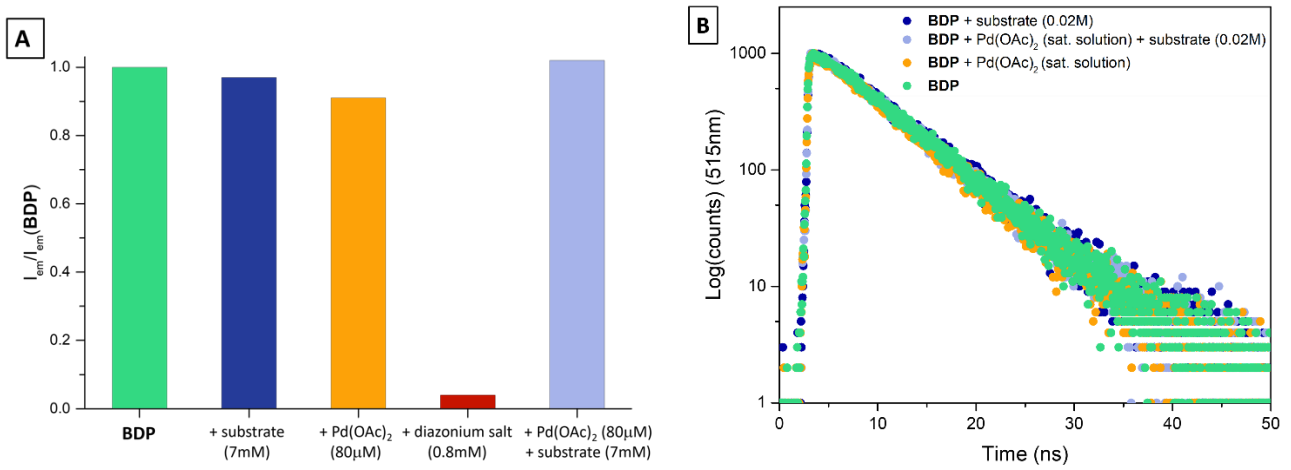

Figure S8. A) Normalized values for singlet oxygen emission sensitized by **BDP** before and after the addition of different quenchers in MeOH:MeCN (1:1, v/v). B) Emission decay profile of **BDP** in the absence (green) and presence of different quenchers in air-equilibrated MeOH, λ_{exc}: 405 nm, λ_{em}: 515nm.

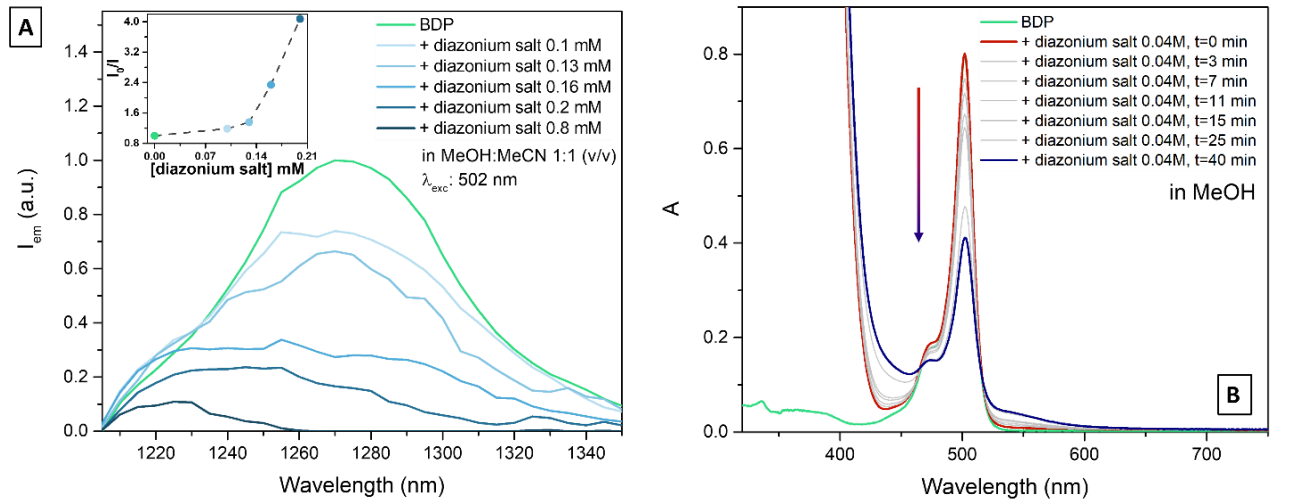

Figure S9. A) Singlet oxygen emission sensitized by **BDP** upon the addition of increasing amounts of diazonium salt (up to 0.8mM); air-equilibrated MeOH:MeCN (1:1, v/v); λ_{exc}: 502nm. Inset: corresponding Stern-Volmer plot. **B)** Absorption spectra showing the side reaction occurring between **BDP** and diazonium salt in aerated MeOH solutions, no light.

We noticed that a side reaction between **BDP** and diazonium salt takes place in air-equilibrated solutions in the dark (**Fig S9-B**). This leads to the degradation of the photosensitizer and explains the non-linearity in the Stern-Volmer plot shown in the inset of **Fig S9-A**. In fact, the higher the concentration of diazonium salt, the faster is the degradation of **BDP** and therefore singlet oxygen emission decreases both due to quenching of T_1 and degradation of PS. Consequently, this does not allow to determine the quenching constant between **BDP** and diazonium salt.

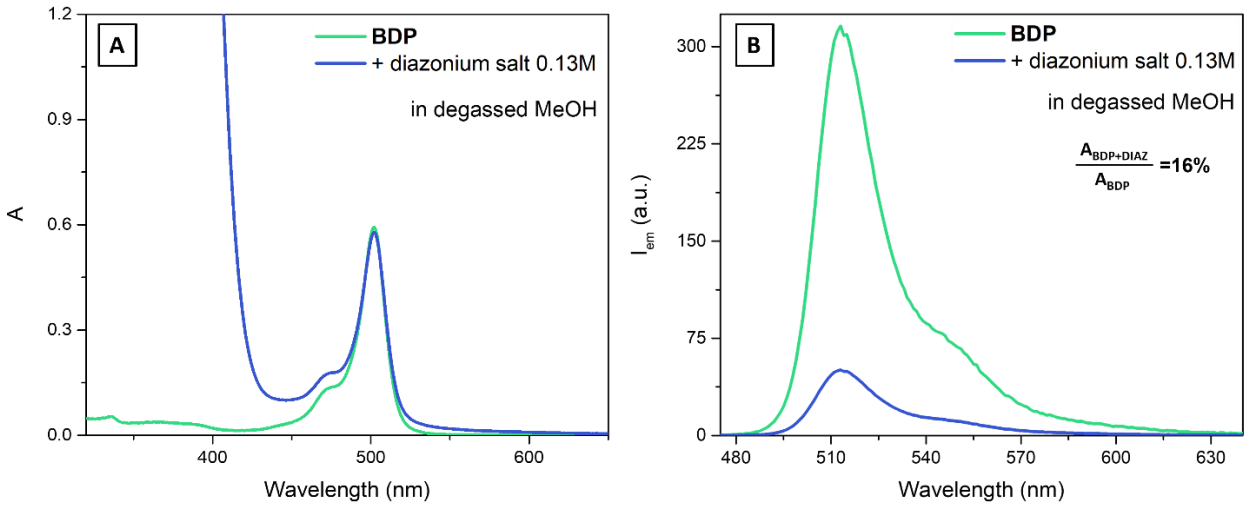

Figure S10. A) Absorption of a **BDP** solution before (green line) and after (blue line) the addition of diazonium salt (0.13M). **B)** Corresponding emission intensity; λ_{exc}: 470 nm; degassed MeOH solution.

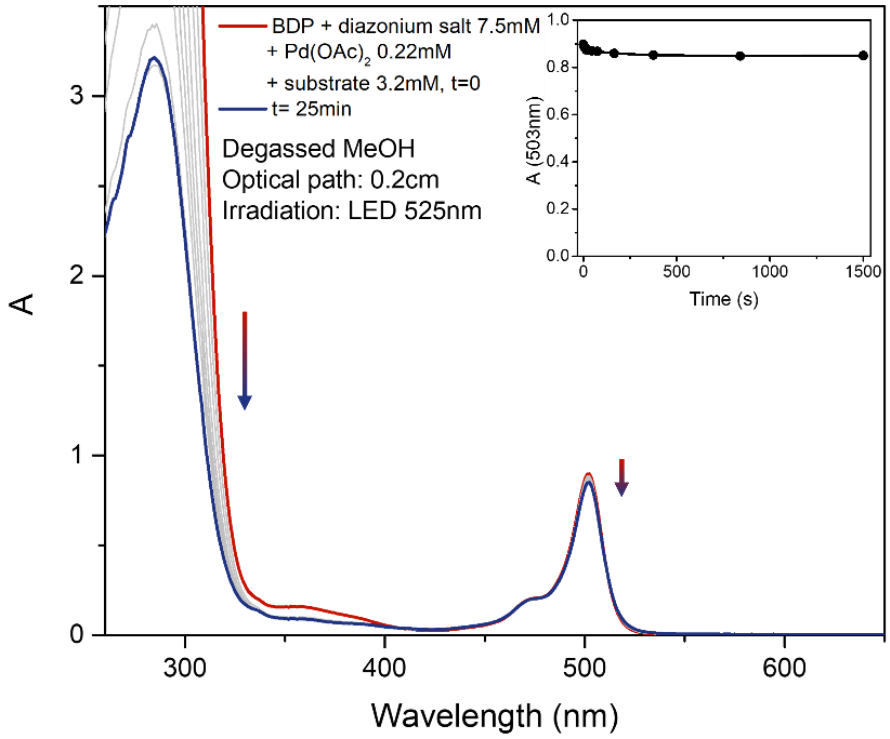

Figure S11. Absorption spectra during irradiation with a 525 nm LED lamp of a degassed MeOH solution containing **BDP** $8x10^{-5}$M, diazonium salt 7.5 mM, substrate 3.2 mM, $Pd(OAc)_2$ 0.22 mM; optical path: 0.2 cm (initial spectrum= red line, final spectrum= blue line). Inset: absorption at 503 nm vs. time.

Computational results

Table S2. Dipole moment (in Debye) of relevant electronic states of **BDP**, calculated in vacuo and in MeCN with TD-M06-2X/6-311G* at S_0 geometry.

(in Debye)	**BDP**	
	vacuo	MeCN
$\mu(S_0)$	5.92	8.07
$\mu(T_1\text{-BDP})$	4.60	6.32
$\mu(S_1\text{-BDP})$	5.27	6.88
$\mu(^1CT)$	16.95	22.67

Cartesian coordinates of optimized geometries. MeCN-M06-2X/6-311G* level of theory.

BDP: ground state

C	-2.505439	2.516700	-0.158225
C	-1.392870	3.357023	0.036435
C	-0.268495	2.559569	0.194337
C	-0.723921	1.213377	0.090501
N	-2.102350	1.239417	-0.121252
H	-1.424858	4.437015	0.059045
B	-3.003400	0.000000	-0.335184
N	-2.102384	-1.239412	-0.121072
C	-2.505509	-2.516688	-0.157914
C	-0.723952	-1.213387	0.090680
C	-1.392974	-3.357022	0.036874
C	-0.268579	-2.559586	0.194728
H	-1.424999	-4.437010	0.059610
F	-4.058481	0.000084	0.581280
F	-3.527000	-0.000086	-1.634814
C	-0.041836	-0.000003	0.186556
C	1.119883	-3.056810	0.450758
H	1.827951	-2.694224	-0.297534
H	1.484677	-2.726843	1.426496

H	1.129163	-4.146783	0.434547
C	-3.930679	-2.901388	-0.364157
H	-4.532142	-2.618955	0.502563
H	-4.347304	-2.385127	-1.230648
H	-4.013811	-3.976528	-0.513530
C	1.120000	3.056755	0.450259
H	1.484806	2.726889	1.426027
H	1.828026	2.694032	-0.298008
H	1.129340	4.146725	0.433908
C	-3.930604	2.901420	-0.364465
H	-4.347279	2.385057	-1.230870
H	-4.532043	2.619124	0.502317
H	-4.013705	3.976543	-0.513978
C	1.435509	0.000016	0.353711
C	2.279349	-0.000086	-0.788716
C	1.974862	0.000161	1.623096
C	1.763836	-0.000225	-2.115306
C	3.690017	-0.000061	-0.607161
C	3.380533	0.000188	1.802955
C	2.611620	-0.000331	-3.191526
H	0.690555	-0.000250	-2.270632
C	4.539825	-0.000173	-1.744421
C	4.206976	0.000077	0.711059
H	3.807303	0.000296	2.796944
C	4.016150	-0.000305	-3.009017
H	2.204222	-0.000438	-4.196133
H	5.614067	-0.000153	-1.590391
H	5.282692	0.000100	0.852347
H	4.670266	-0.000391	-3.872951
O	1.092975	0.000258	2.651529
C	1.601466	0.000378	3.978187
H	2.198810	0.894549	4.170049

H	0.730129	0.000434	4.626993
H	2.198815	-0.893754	4.170211

BDP: 3CT state

C	2.129649	-2.692200	0.739735
C	0.940977	-3.234428	1.216271
C	-0.077086	-2.283305	1.050574
C	0.529809	-1.169732	0.421523
N	1.880798	-1.441481	0.271141
H	0.832067	-4.214268	1.660508
B	2.969588	-0.437700	-0.147609
N	2.277705	0.919110	-0.370581
C	2.889859	2.019681	-0.881968
C	0.912020	1.145685	-0.340610
C	1.919493	2.963654	-1.204566
C	0.662544	2.424322	-0.897346
H	2.110117	3.933221	-1.643529
F	3.950720	-0.332795	0.853741
F	3.600088	-0.862204	-1.333254
C	0.017813	0.122145	0.083630
C	-0.648153	3.076257	-1.210975
H	-1.375260	2.364950	-1.610672
H	-1.104258	3.553838	-0.338639
H	-0.500220	3.853518	-1.961918
C	4.369921	2.101082	-1.048740
H	4.879211	1.973649	-0.090987
H	4.730133	1.311641	-1.711602
H	4.646792	3.067897	-1.467347
C	-1.484131	-2.461297	1.535919
H	-1.885421	-1.548111	1.982553
H	-2.171630	-2.757517	0.738022

H	-1.507742	-3.242088	2.297487
C	3.497279	-3.289152	0.732785
H	3.965305	-3.180862	-0.247605
H	4.145607	-2.788568	1.455291
H	3.444498	-4.347676	0.985114
C	-1.391639	0.381546	0.166447
C	-2.359974	-0.398727	-0.559852
C	-1.888620	1.449803	1.045936
C	-1.965689	-1.312571	-1.548369
C	-3.750010	-0.193769	-0.323472
C	-3.248762	1.658001	1.222635
C	-2.910042	-2.084032	-2.228110
H	-0.914581	-1.420256	-1.785142
C	-4.677768	-0.987124	-1.000756
C	-4.166597	0.840711	0.575560
H	-3.604268	2.420916	1.901637
C	-4.259186	-1.936628	-1.939142
H	-2.584775	-2.790560	-2.981328
H	-5.735108	-0.852209	-0.801671
H	-5.226936	0.990956	0.739311
H	-4.996366	-2.539787	-2.455319
O	-0.931364	2.094651	1.699213
C	-1.293747	3.157821	2.576981
H	-1.903928	2.780500	3.399072
H	-0.358393	3.555046	2.957429
H	-1.836416	3.932201	2.030835

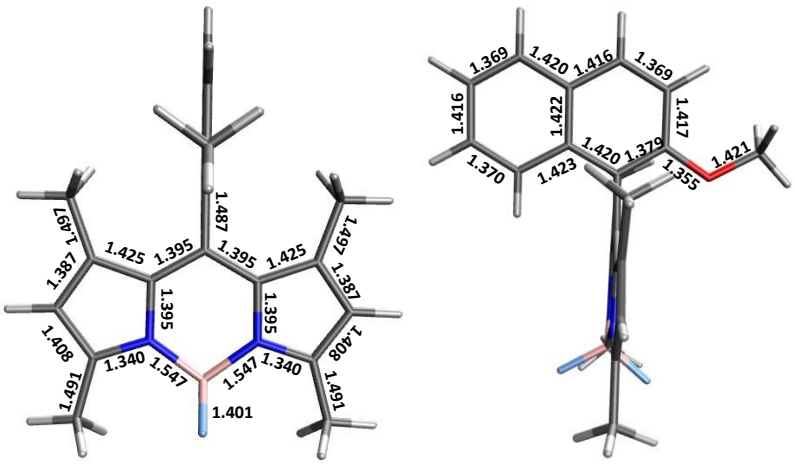

Figure S12. Bond lengths of BDP's ground state geometry optimized at MeCN-M06-2X/6-311G* level of theory. (left) BODIPY core; (right) the 2-methoxynaphthalene unit. C-H bond lengths are omitted for clarity.

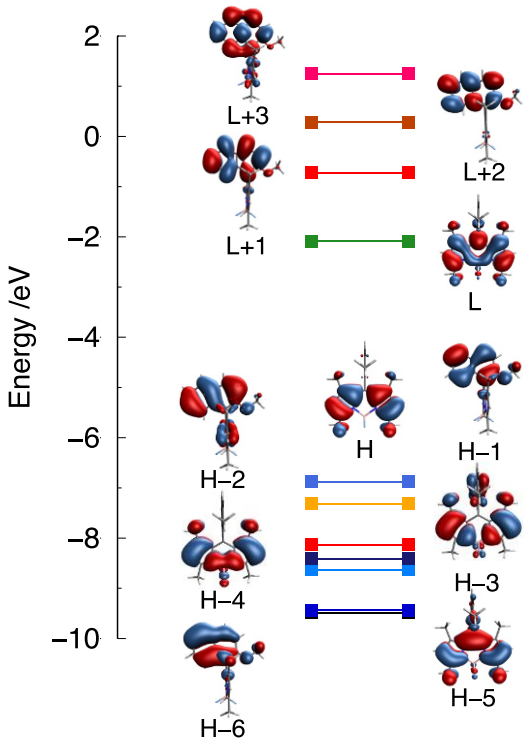

Figure S13. Energies and shapes of molecular orbitals involved in the excited states of **BDP**. MeCN-M06-2X/6-311G* calculations.

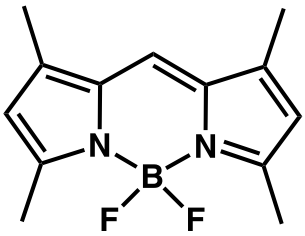

Figure S14. Boron dipyrromethene chosen as model molecule for the comparison of frontier molecular orbital energies and redox potentials.

Table S3. Comparison between calculated frontier molecular orbital (MO) energies and redox potentials of **BDP** and boron dipyrromethene. MO energies are calculated with MeCN-M06-2X/6-311G* level of theory.

orbital	Energy BDP / eV	Energy Boron dipyrromethene / eV	Redox BDP This work / V	Redox Boron dipyrromethene ref [19] / V
L	-1.75	-1.98	-1.15	-1.19
H	-6.52	-6.70	+1.15	+1.21

Accurate computational predictions of redox potentials require comparison of energies for both the starting molecule and its reduced/oxidized forms. However, we can qualitatively use Koopmans' theorem[34] to correlate the redox potentials of BODIPY derivatives with H/L computed energies. To this end we can compare computed orbitals energies of **BDP** with those of the reference boron dipyrromethene. Both HOMO and LUMO energies of **BDP** are slightly higher than those of boron dipyrromethene (see **Table S3**) which is in agreement with the modest changes in redox potentials determined for **BDP**.

Table S4. Excitation energies, wavefunction analysis, oscillator strength and assignment to the experimental spectrum of the singlet excited states of **BDP** at the ground state geometry. The excitation energies to the two lowest triplet states are also included. TD-M06-2X/6-311G* calculations in vacuo.

BDP					
State	**Exc. E (eV)**	**λ(nm)**	**Wavefunction**	**Osc. strength**	**Band #**
T_1-B[a]	1.51	822	0.72 (H → L)	0	
S_1-B[a]	2.99	414	0.70 (H → L)	0.505	1
^{3}CT	3.44	361	0.69(H-1 → L)	0	
^{1}CT	3.45	360	0.69 (H-1 → L)	0.0005	
S_2-B[a]/N[b]	3.94	315	0.65 (H-2 → L)	0.0499	2
^{1}CT (2)	4.16	298	0.70 (H → L+1)	0.0089	
S_3-B[a]	4.22	294	0.70 (H-4 → L)	0.0311	
S_1-N[b]	4.34	285	0.62 (H-1 → L+1) 0.45 (H-6 → L+1)	0.1211	3
^{1}CT (3)	4.71	263	0.65 (H-3 → L)	0.0032	
S_2-N[b]	4.76	261	0.42 (H-1 → L+2) -0.41 (H-2 → L+1)	0.0436	4
^{1}CT (4)	5.22	238	0.70 (H → L+2)	0.0049	
S_4-B[a]	5.41	229	0.67 (H-5 → L) 0.11 (H-1 → L+2)	0.3863	5

[a] B = excited states localized on BODIPY subunit; [b] N = excited states localized on the 2-methoxynaphthalene subunit.

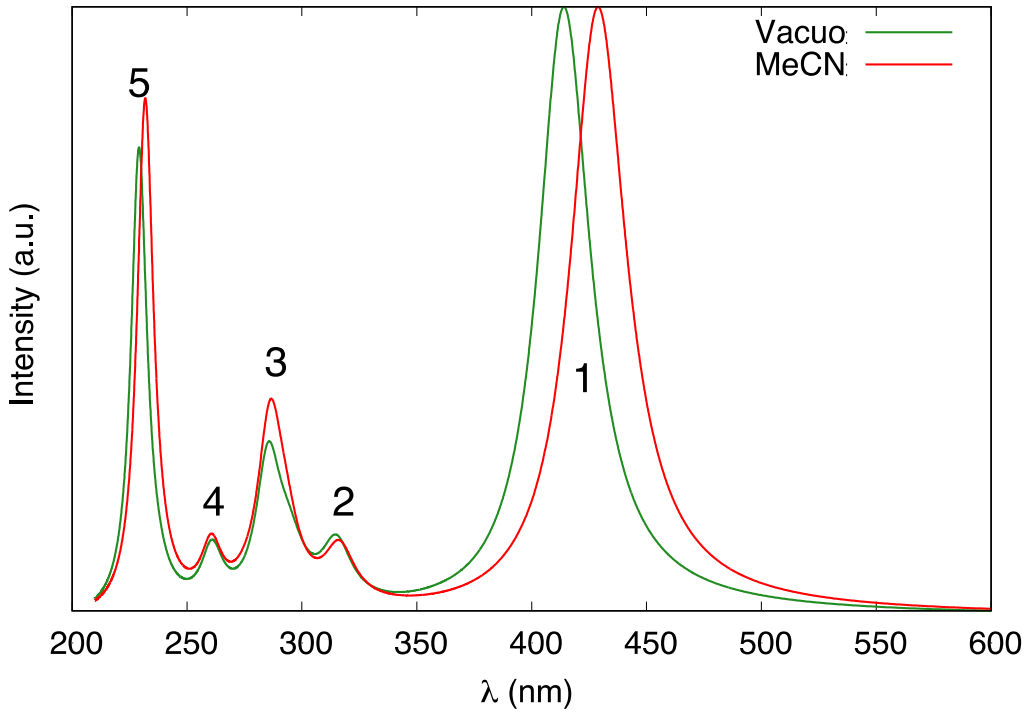

Figure S15. Comparison between calculate absorption spectra of **BDP**. Red spectrum: MeCN-TD-M06-2X/6-311G* calculations; green spectrum: TD-M06-2X/6-311G* calculation. Absorption intensities are normalized w.r.t the intensity of the first band, respectively. Numbers in the plot correspond to the number of band shown in **Table S4.**

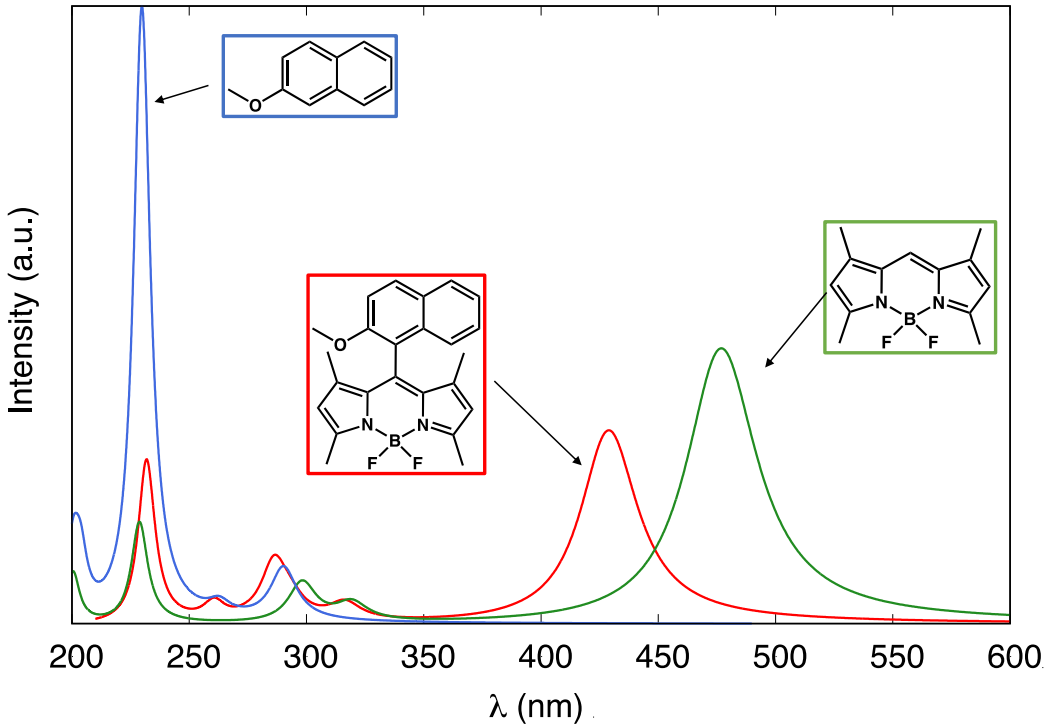

Figure S16. Absorption spectra of **BDP** (red) and the two subunits: boron dipyrromethene (green) and 2-methoxynaphthalene (blue). From MeCN-TD-M06-2X/6-311G* calculations.

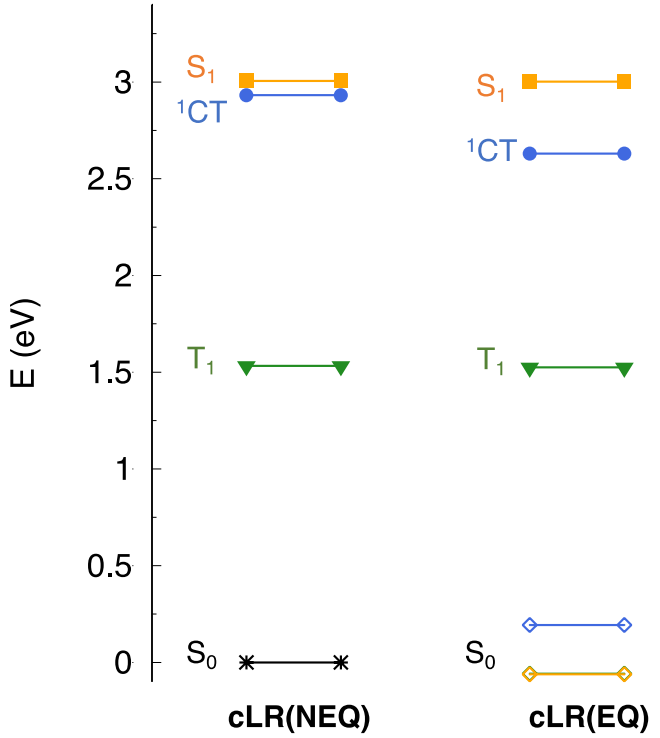

Figure S17. Excited states pattern of **BDP** calculated at the ground state geometry including solvent corrections. (left) cLR(NEQ) correction: only the fast solvent component is equilibrated on the corresponding excited state; (right) cLR(EQ) correction: here, solvent components are fully equilibrated on the corresponding excited state. S_0 can be destabilized or stabilized accordingly. Color codes of S_0 cLR(EQ) reflect the excited state on which the solvent is stabilized.

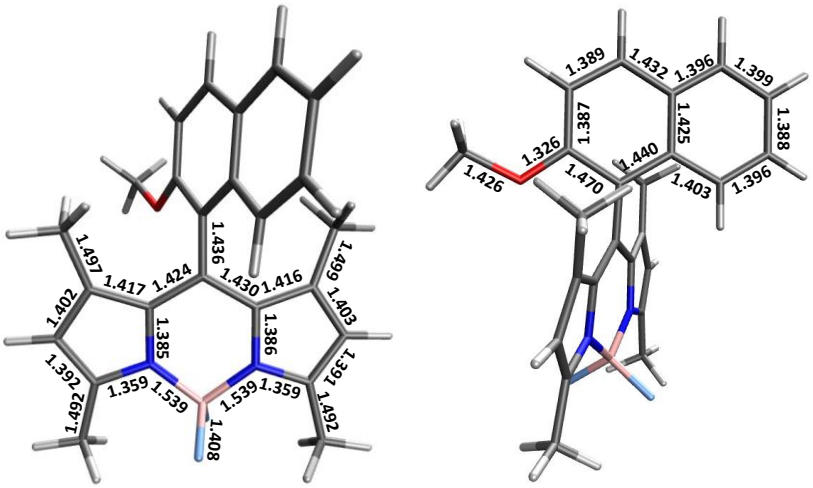

Figure S18. Bond lengths of the optimized geometry of the ^{3}CT state at MeCN-LR-TD-M06-2X/6-311G* level of theory. C-H bond lengths are omitted for clarity.

References

[1] J. Park, S. Chang, *Angew. Chem.* **2015**, *127*, 14309–14313.

[2] J. L. Bolliger, C. M. Frech, *Adv. Synth. Catal.* **2010**, *352*, 1075–1080.

[3] Y. Zhang, Y. Zhao, Y. Luo, L. Xiao, Y. Huang, X. Li, Q. Peng, Y. Liu, B. Yang, C. Zhu, X. Zhou, J. Zhang, *Org. Lett.* **2017**, *19*, 6470–6473.

[4] J. K. Laha, K. P. Jethava, S. Patel, *Org. Lett.* **2015**, *17*, 5890–5893.

[5] T. Mino, Y. Harada, H. Shindo, M. Sakamoto, T. Fujita, *Synlett* **2008**, *2008*, 614–620.

[6] M. P. Huestis, L. Chan, D. R. Stuart, K. Fagnou, *Angew. Chem.* **2011**, *123*, 1374–1377.

[7] M. Taillefer, N. Xia, A. Ouali, *Angew. Chem.* **2007**, *119*, 952–954.

[8] M. Chen, X. Zheng, W. Li, J. He, A. Lei, *J. Am. Chem. Soc.* **2010**, *132*, 4101–4103.

[9] Q.-L. Yang, Y. Liu, L. Liang, Z.-H. Li, G.-R. Qu, H.-M. Guo, *J. Org. Chem.* **2022**, *87*, 6161–6178.

[10] P. Hanson, J. R. Jones, A. B. Taylor, P. H. Walton, A. W. Timms, *J. Chem. Soc., Perkin Trans. 2* **2002**, 1135–1150.

[11] M. Montalti, A. Credi, L. Prodi, M. T. Gandolfi, *Handbook of Photochemistry*, CRC Press, **2006**.

[12] F. WilkinsonW, *J. Phys. Chem. Ref. Data* **1993**, *22*, 113–262.

[13] J. Tomasi, B. Mennucci, R. Cammi, *Chem. Rev.* **2005**, *105*, 2999–3094.

[14] V. Postils, F. Ruipérez, D. Casanova, *J. Chem. Theory Comput.* **2021**, *17*, 5825–5838.

[15] F. Zinna, T. Bruhn, C. A. Guido, J. Ahrens, M. Bröring, L. Di Bari, G. Pescitelli, *Chem. Eur. J.* **2016**, *22*, 16323–16323.

[16] S. Chibani, A. D. Laurent, B. Le Guennic, D. Jacquemin, *J. Chem. Theory Comput.* **2014**, *10*, 4574–4582.

[17] S. Chibani, B. Le Guennic, A. Charaf-Eddin, A. D. Laurent, D. Jacquemin, *Chem. Sci.* **2013**, *4*, 1950.

[18] A. Charaf-Eddin, B. Le Guennic, D. Jacquemin, *RSC Adv.* **2014**, *4*, 49449–49456.

[19] M. A. Filatov, S. Karuthedath, P. M. Polestshuk, S. Callaghan, K. J. Flanagan, M. Telitchko, T. Wiesner, F. Laquai, M. O. Senge, *Phy. Chem. Chem. Phy.* **2018**, *20*, 8016–8031.

[20] M. A. Filatov, S. Karuthedath, P. M. Polestshuk, S. Callaghan, K. J. Flanagan, T. Wiesner, F. Laquai, M. O. Senge, *ChemPhotoChem* **2018**, *2*, 606–615.

[21] M. A. Filatov, *Org. Bio. Chem.* **2020**, *18*, 10–27.

[22] E. Bassan, Y. Dai, D. Fazzi, A. Gualandi, P. G. Cozzi, F. Negri, P. Ceroni, *Photochem. Photobiol. Sci.* **2022**, 1–10.

[23] M. Laine, N. A. Barbosa, R. Wieczorek, M. Y. Melnikov, A. Filarowski, *J. Mol. Model.* **2016**, *22*, 1–7.

[24] B. Mennucci, *Int. J. Quantum Chem.* **2015**, *115*, 1202–1208.

[25] M. Caricato, B. Mennucci, J. Tomasi, F. Ingrosso, R. Cammi, S. Corni, G. Scalmani, *The Journal of chemical physics* **2006**, *124*, 124520.

[26] M. J. Frisch, G. W. Trucks, H. B. Schlegel, G. E. Scuseria, M. A. Robb, J. R. Cheeseman, G. Scalmani, V. Barone, G. A. Petersson, H. Nakatsuji, X. Li, M. Caricato, A. V Marenich, J. Bloino, B. G. Janesko, R. Gomperts, B. Mennucci, H. P. Hratchian, J. . Ortiz, A. F. Izmaylov, J. L. Sonnenberg, D. Williams-Young, F. Ding, F. Lipparini, F. Egidi, J. Goings, B. Peng, A. Petrone, T. Henderson, D. Ranasinghe, V. G. Zakrzewski, J. Gao, N. Rega, G. Zheng, W. Liang, M. Hada, M. Ehara, K. Toyota, R. Fukuda, J. Hasegawa, M. Ishida, T. Nakajima, Y. Honda, O. Kitao, H. Nakai, T. Vreven, K. Throssell, J. A. Montgomery, Jr., J. E. Peralta, F. Ogliaro, M. J. Bearpark, J. J. Heyd, E. N. Brothers, K. N. Kudin, V. N. Staroverov, T. A. Keith, R. Kobayashi, J. Normand, K. Raghavachari, A. P. Rendell, J. C. Burant, S. S. Iyengar, J. Tomasi, M. Cossi, J. M. Millam, M. Klene, C. Adamo, R. Cammi, J. W. Ochterski, R. L. Martin, K. Morokuma, O. Farkas, J. B. Foresman, D. J. Fox, *Gaussian Inc.: Wallingford, CT* **2016**.

[27] B. de Souza, G. Farias, F. Neese, R. Izsak, *J. Chem. Theory Comput.* **2019**, *15*, 1896–1904.

[28] F. Neese, *The Journal of chemical physics* **2005**, *122*, 034107.
[29] E. Van Lenthe, J. G. Snijders, E. J. Baerends, *The Journal of chemical physics* **1996**, *105*, 6505–6516.
[30] F. Neese, F. Wennmohs, U. Becker, C. Riplinger, *The Journal of chemical physics* **2020**, *152*, 224108.
[31] S. Banfi, G. Nasini, S. Zaza, E. Caruso, *Tetrahedron* **2013**, *69*, 4845–4856.
[32] K. Korvorapun, J. Struwe, R. Kuniyil, A. Zangarelli, A. Casnati, M. Waeterschoot, L. Ackermann, *Angewandte Chemie International Edition* **2020**, *59*, 18103–18109.
[33] D. Xue, J. Li, Y.-X. Liu, W.-Y. Han, Z.-T. Zhang, C. Wang, J. Xiao, *Synlett* **2012**, *23*, 1941–1946.
[34] T. Koopmans, *Physica* **1934**, *1*, 104–113.

Copies of NMR Spectra

Figure S19. ^{1}H NMR (401 MHz, $CDCl_3$) for **1, BDP**

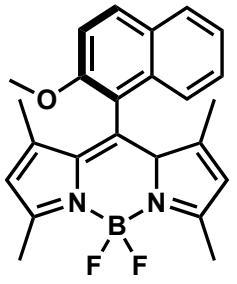

1, BDP

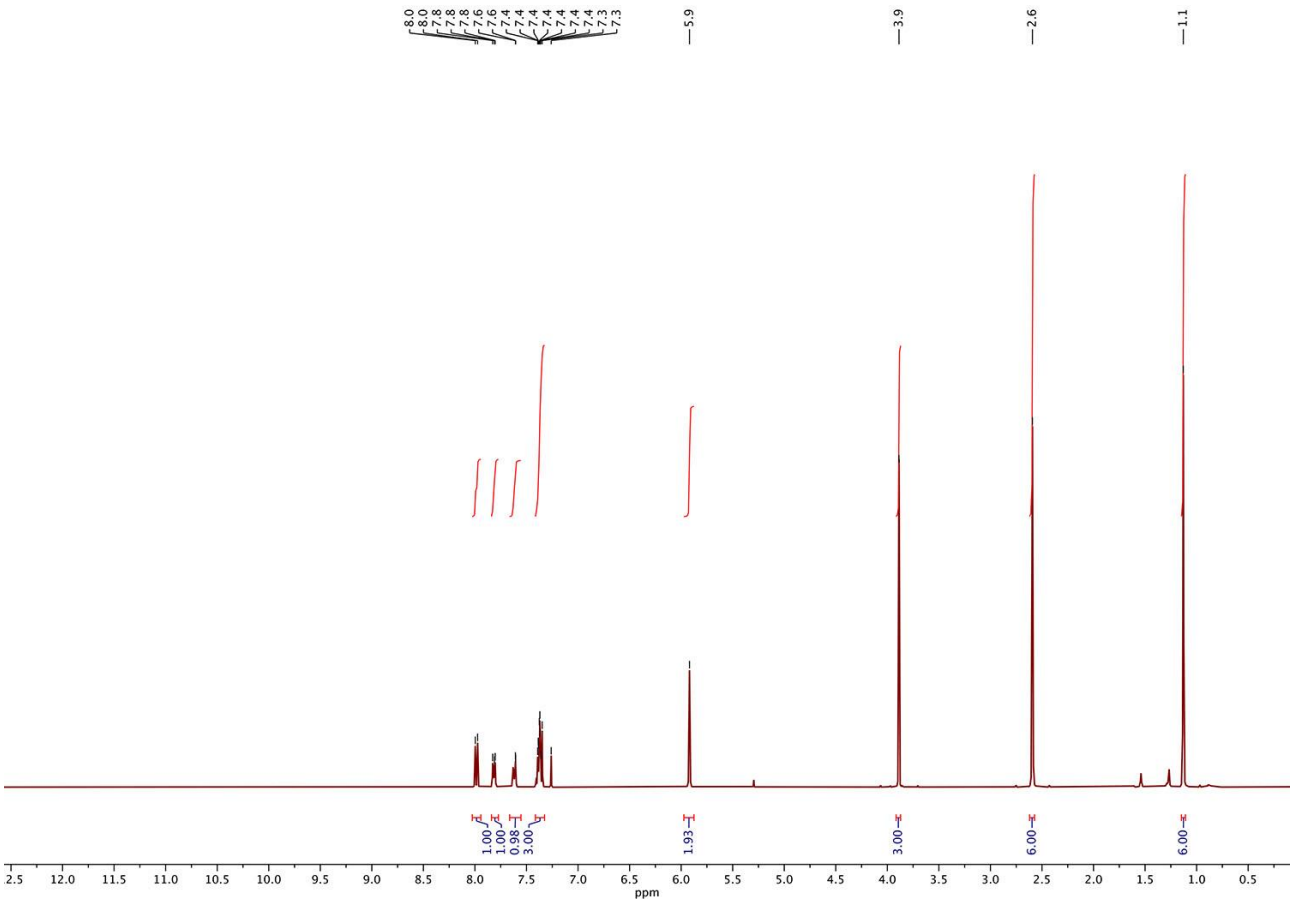

Figure S20. $^{13}C\{^{1}H\}$ NMR (101 MHz, $CDCl_3$) for **1, BDP**

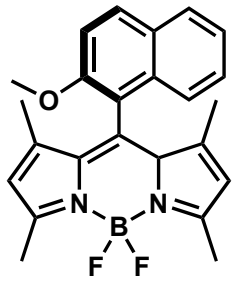

1, **BDP**

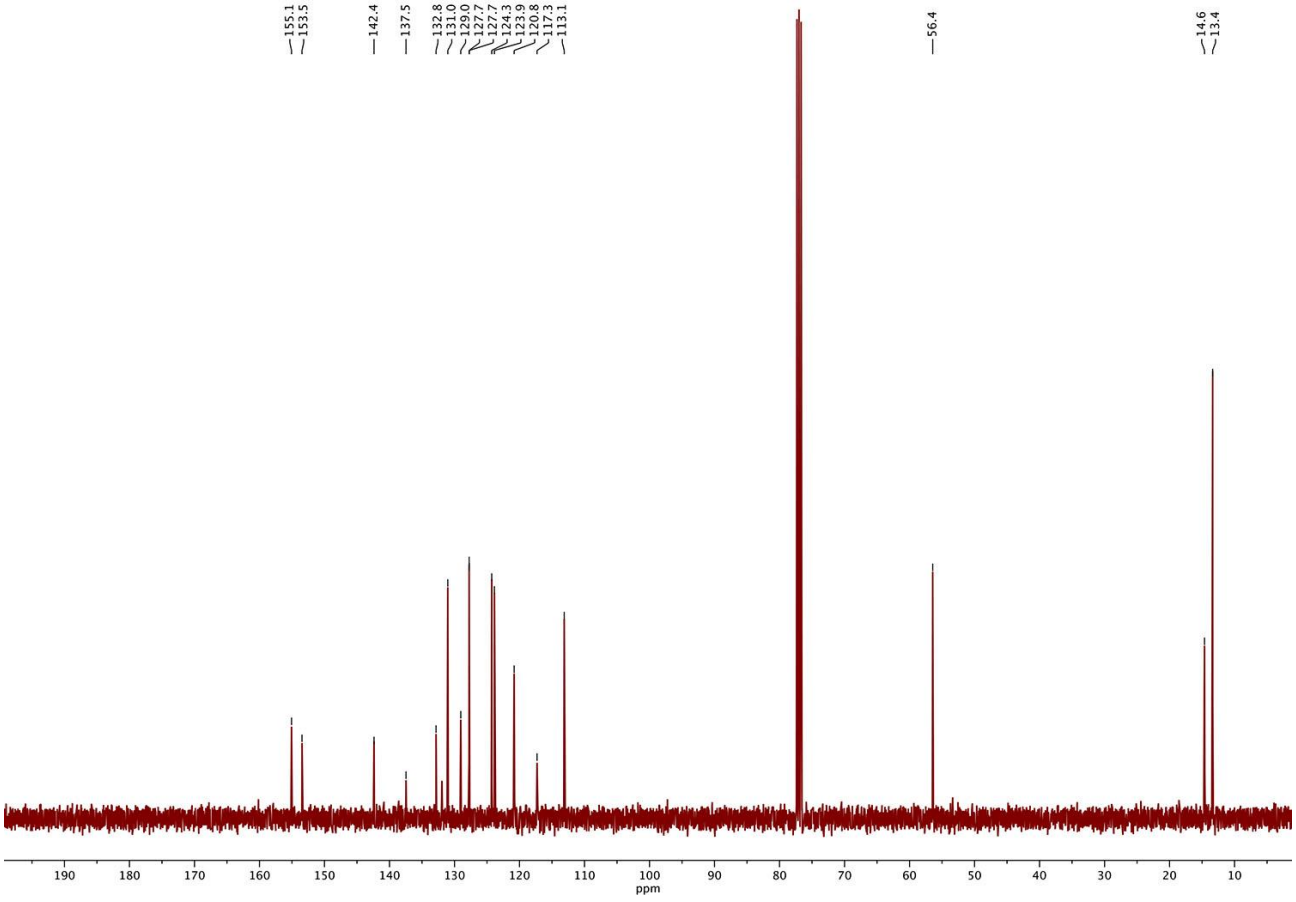

Figure S21. ^{19}F NMR (376.5 Hz, $CDCl_3$) for **1, BDP**

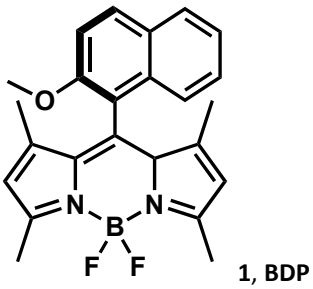

1, BDP

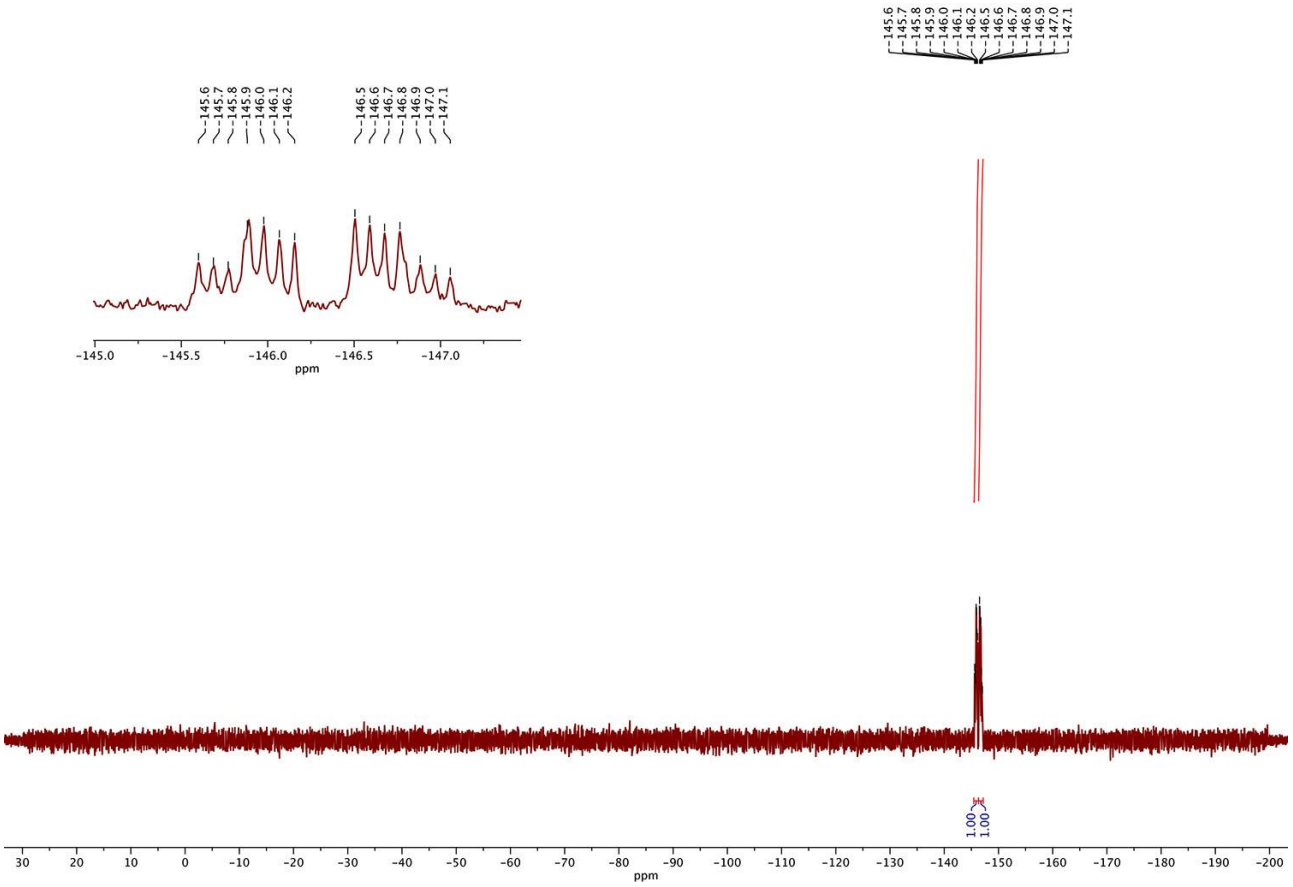

Figure S22. ^{1}H NMR (401 MHz, $CDCl_3$) for **4a**

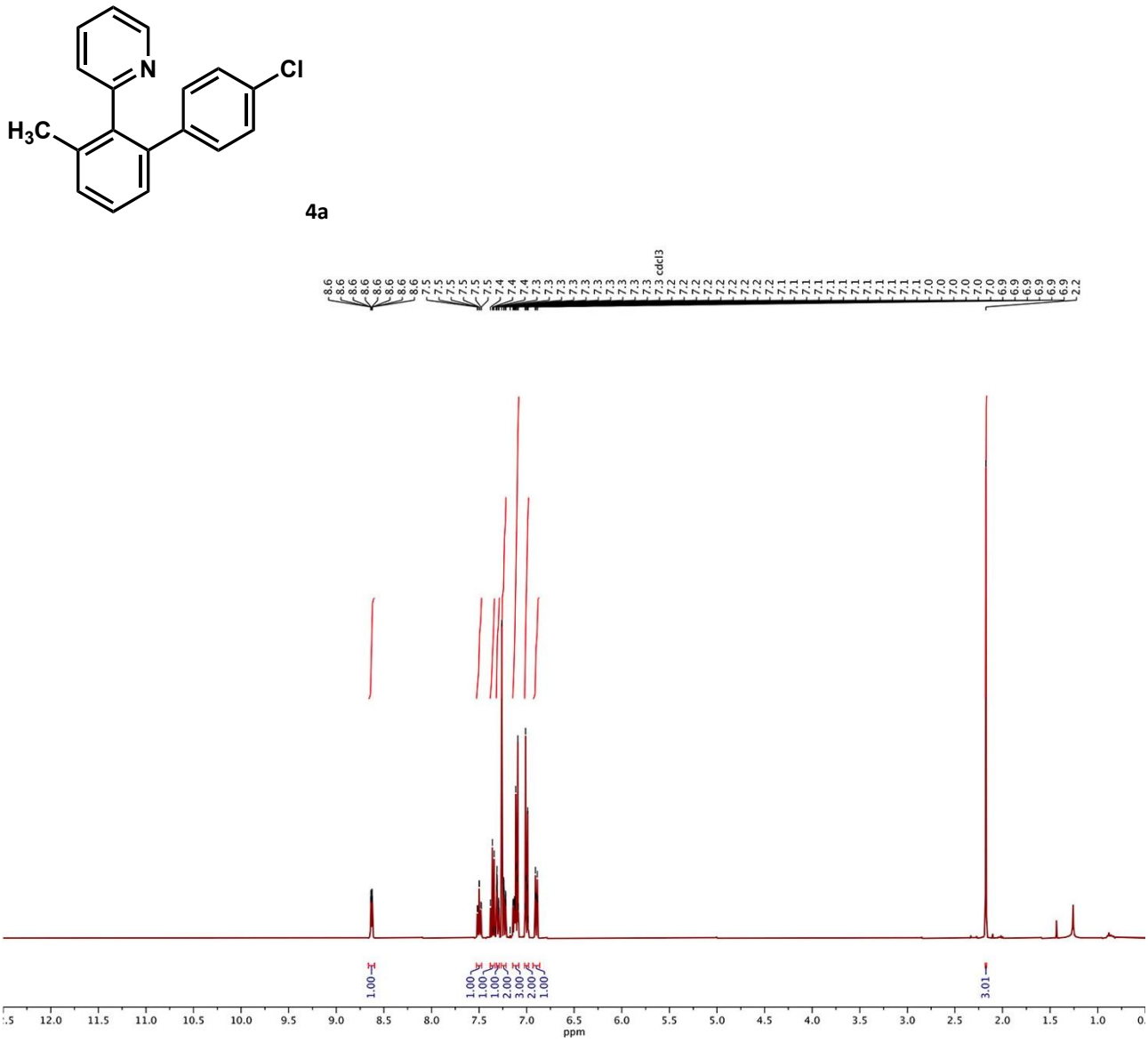

Figure S23. $^{13}C\{^{1}H\}$ NMR (101 MHz, $CDCl_3$) for **4a**

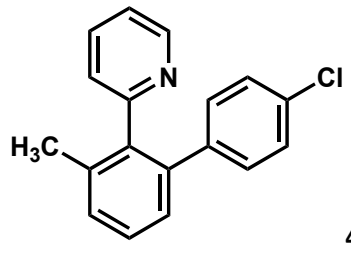

4a

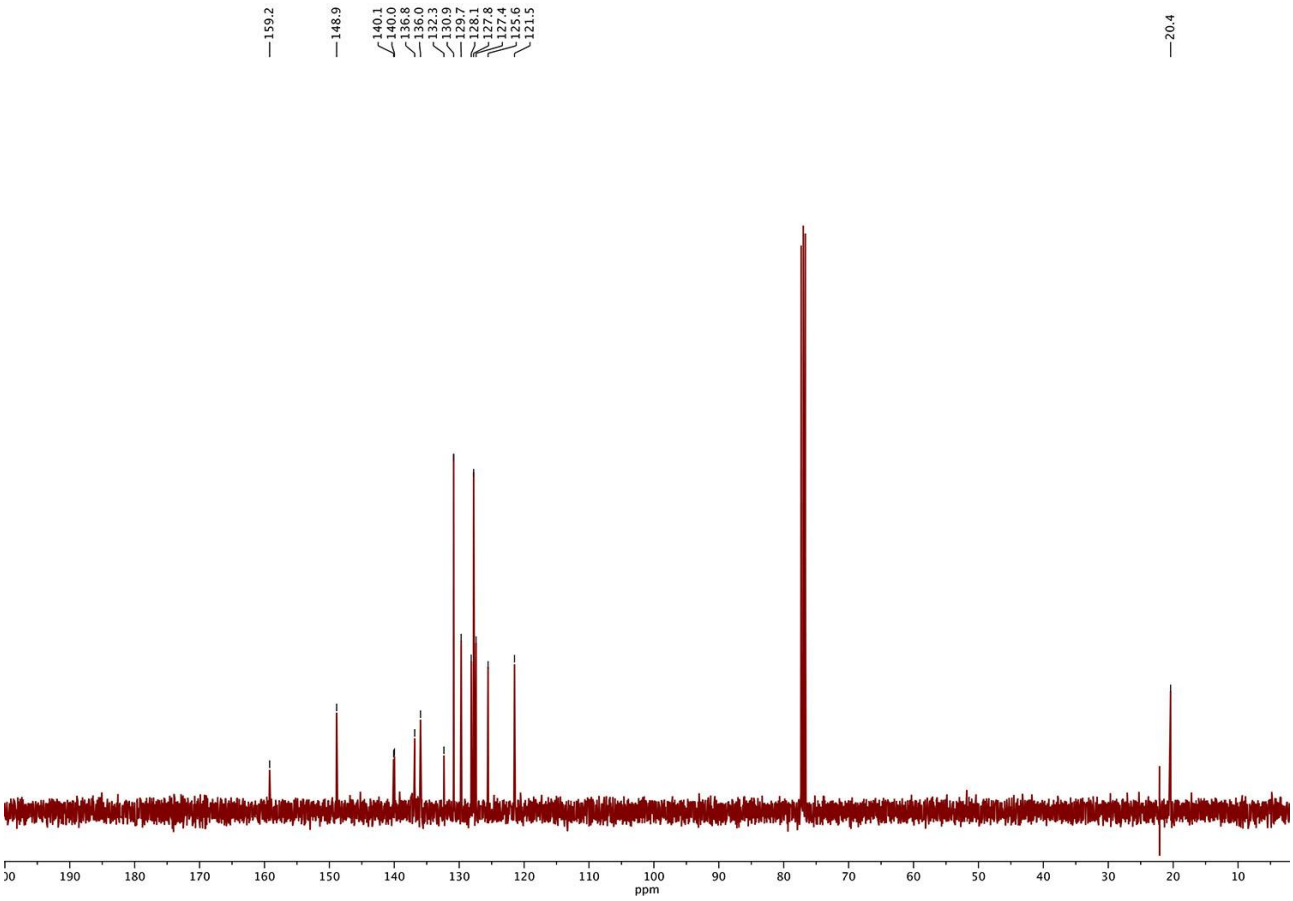

Figure S24. ^{1}H NMR (401 MHz, $CDCl_3$) for **4b**

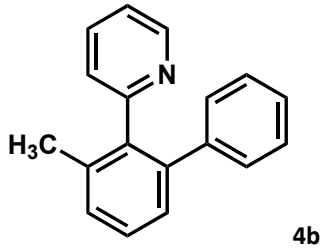

4b

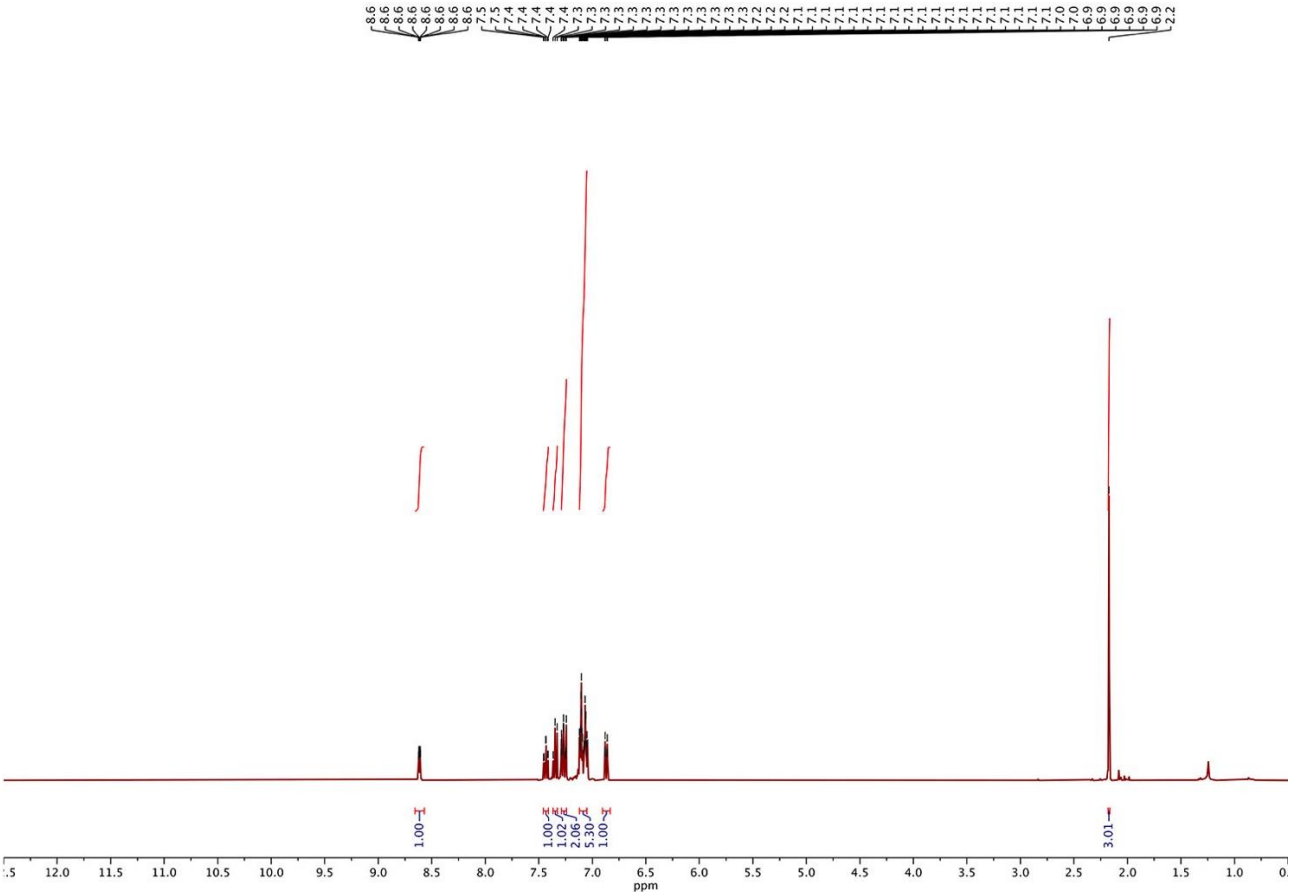

Figure S25. $^{13}C\{^{1}H\}$ NMR (101 MHz, $CDCl_3$) for **4b**

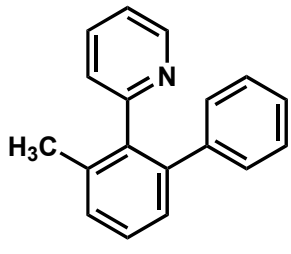

4b

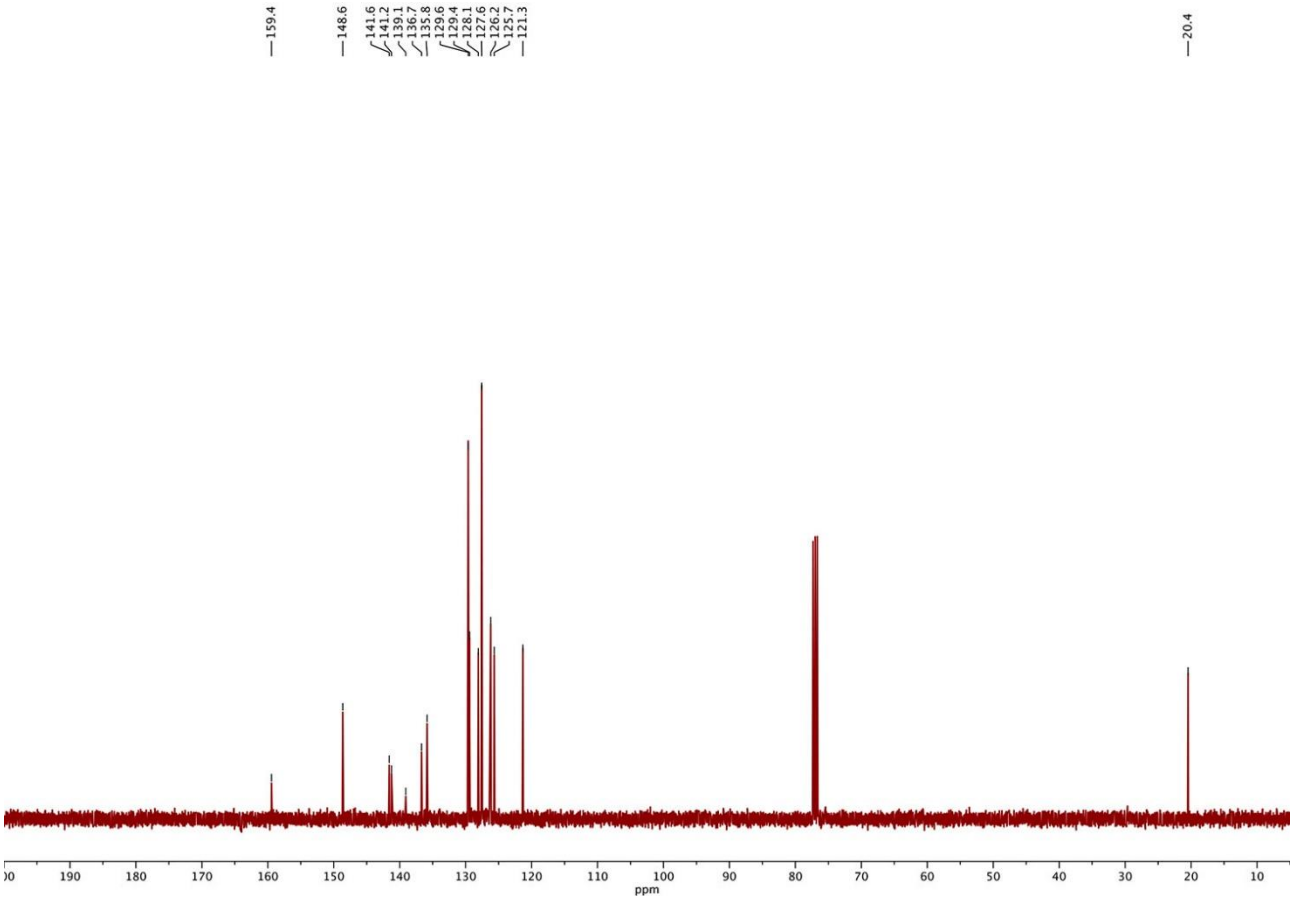

Figure S26. ^{1}H NMR (401 MHz, $CDCl_3$) for **4c**

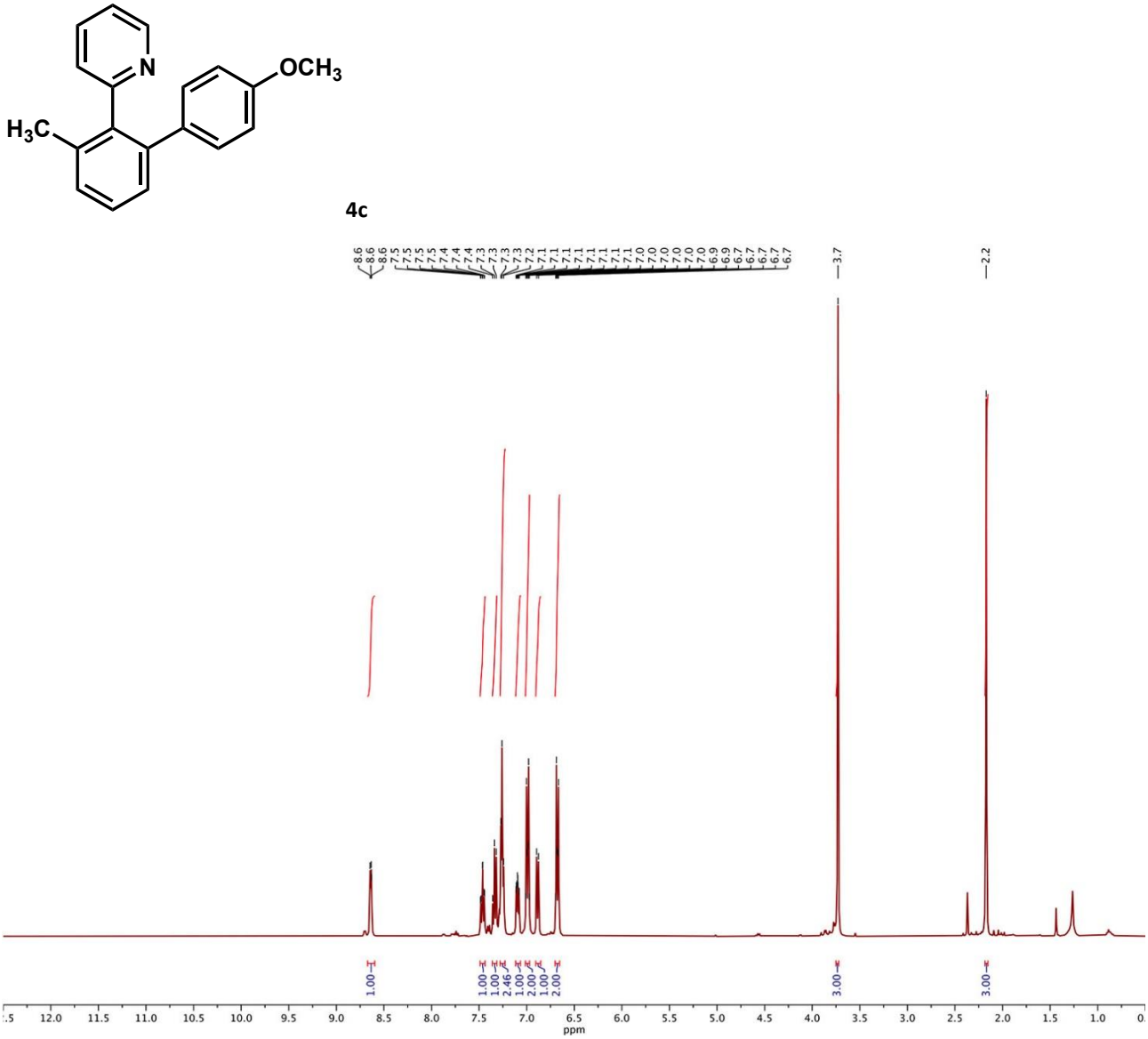

Figure S27. $^{13}C\{^{1}H\}$ NMR (101 MHz, $CDCl_3$) for **4c**

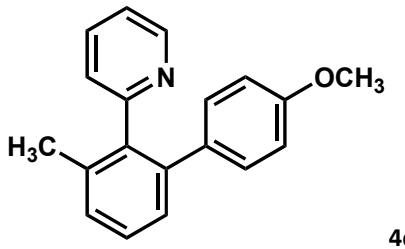

4c

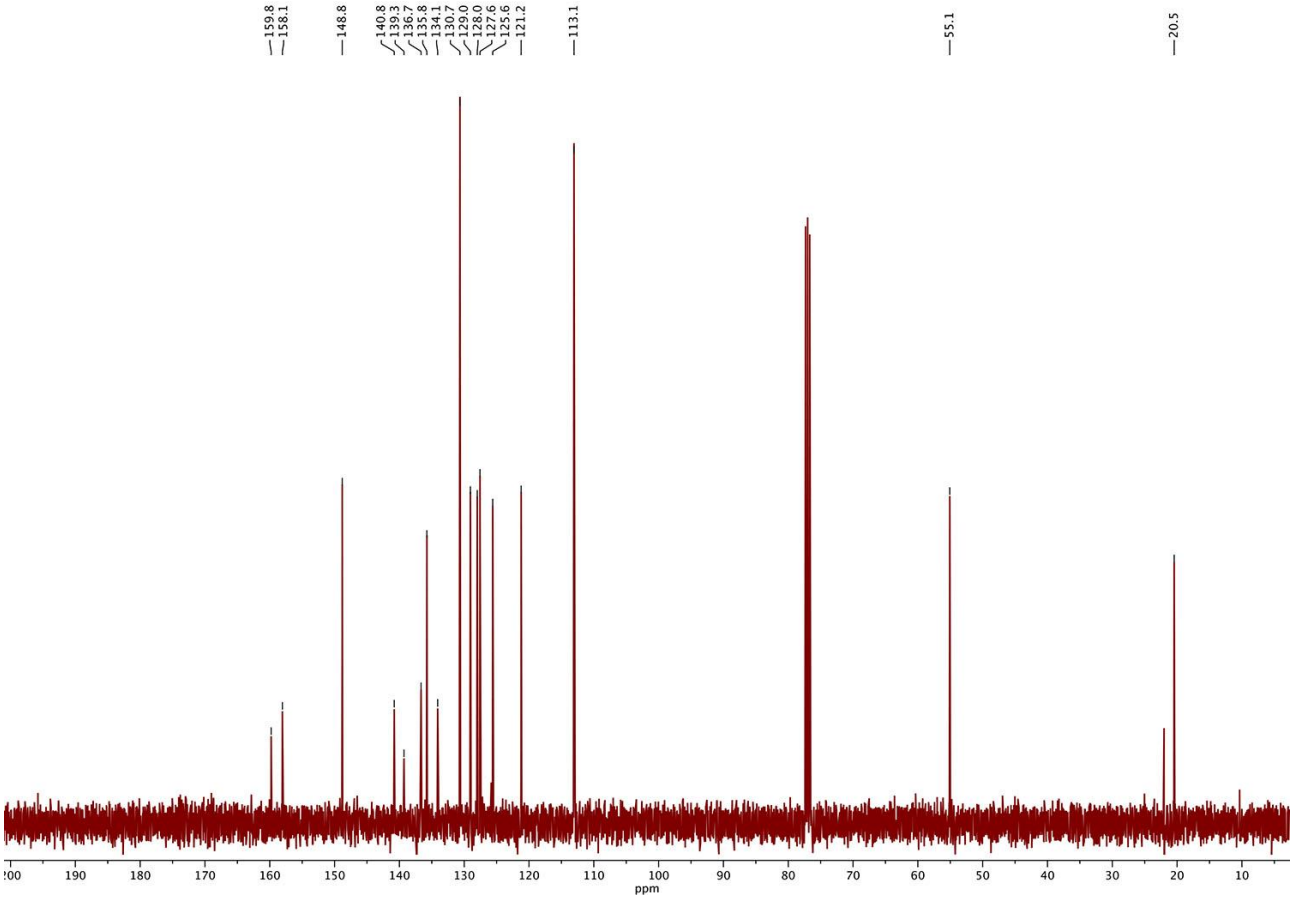

Figure S28. ^{1}H NMR (401 MHz, $CDCl_3$) for **4d**

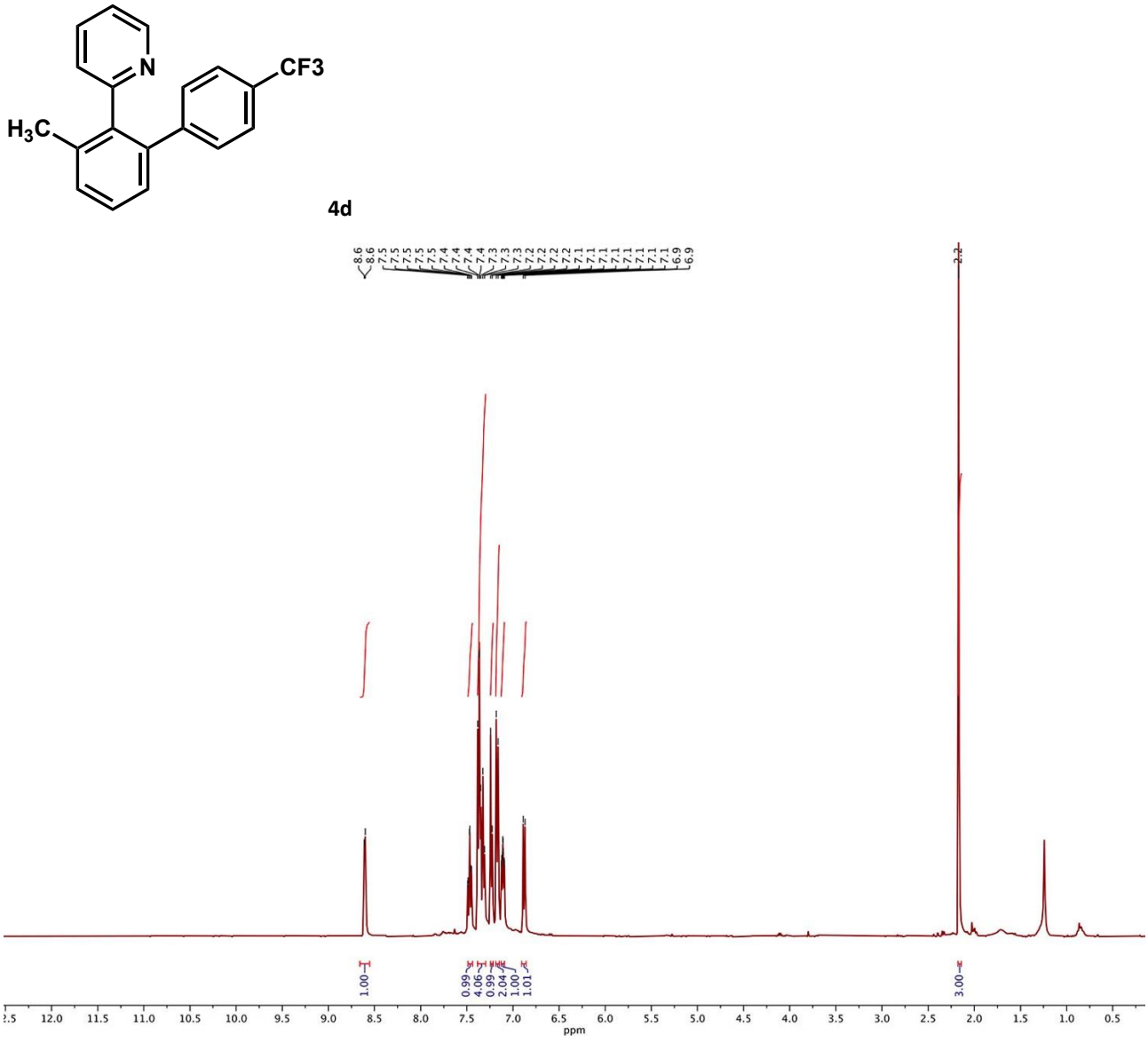

Figure S29. $^{13}C\{^{1}H\}$ NMR (101 MHz, $CDCl_3$)for **4d**

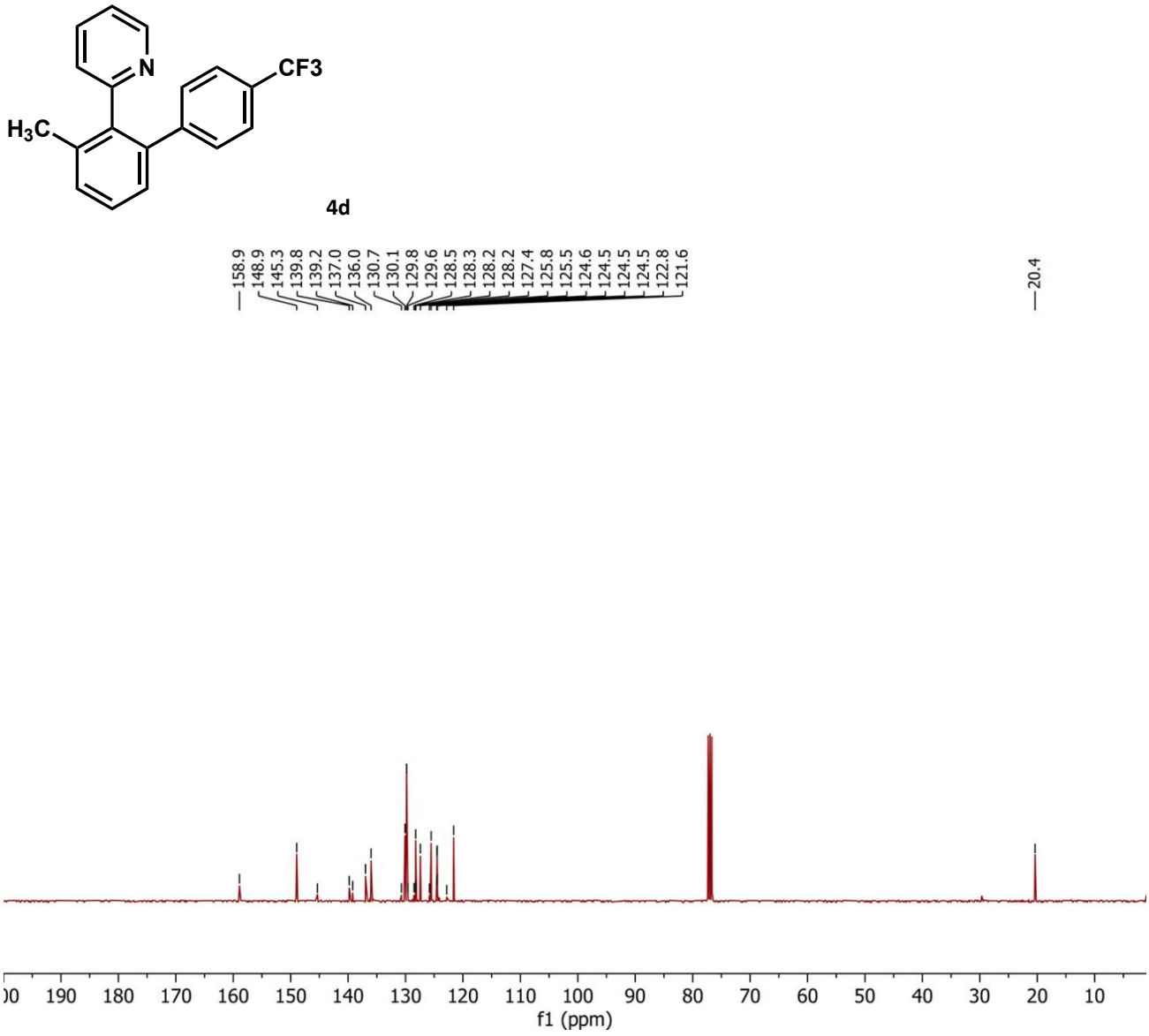

Figure S30. ^{19}F NMR (376.5 Hz, $CDCl_3$) for **4d**

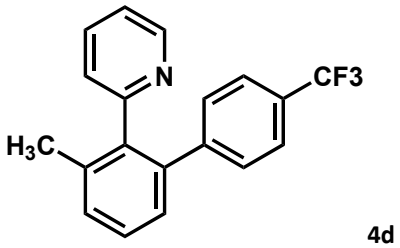

4d

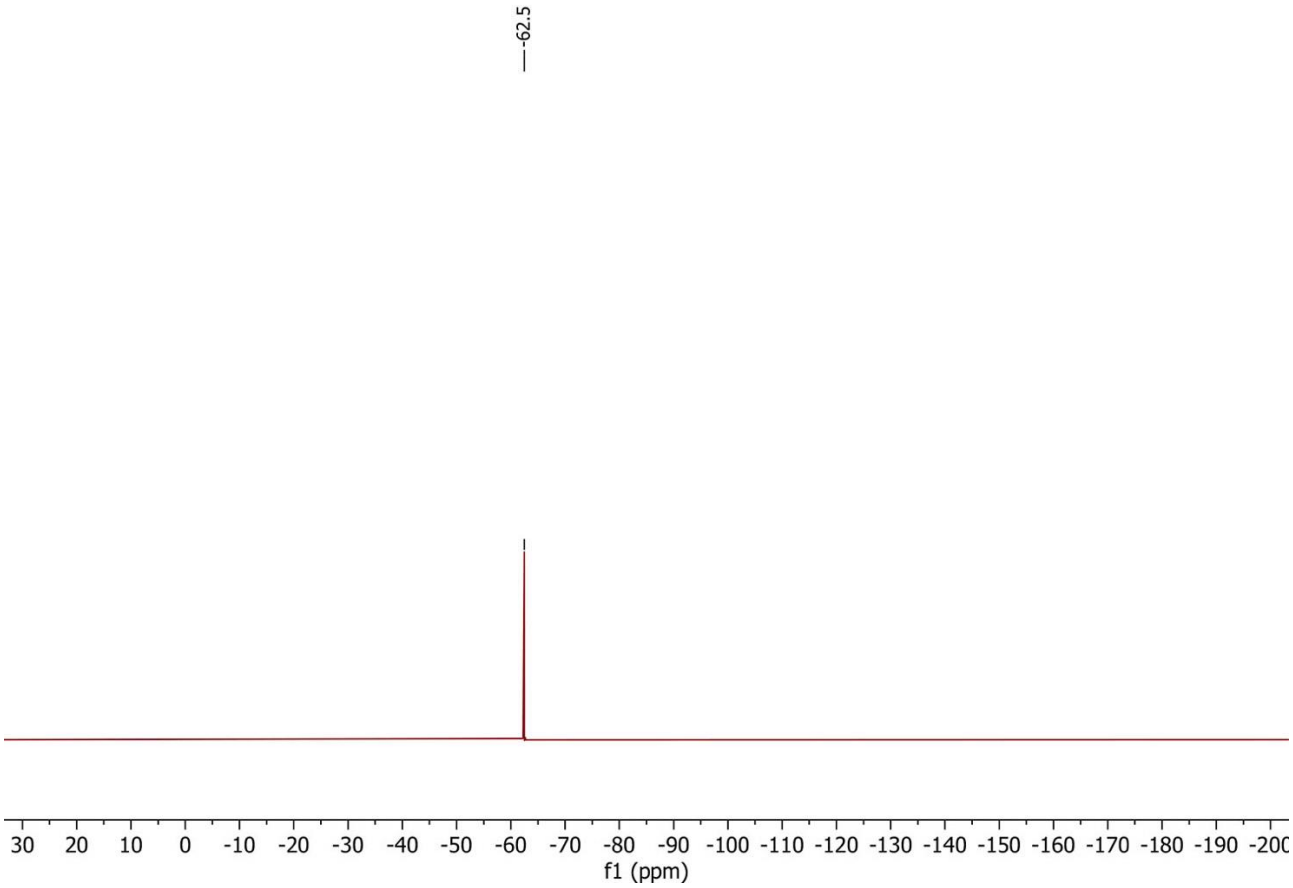

Figure S31. ^{1}H NMR (401 MHz, $CDCl_3$) for **4e**

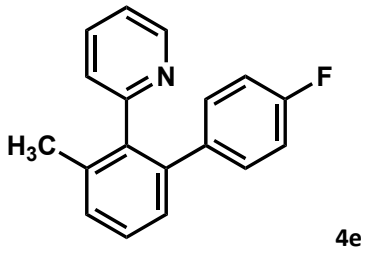

4e

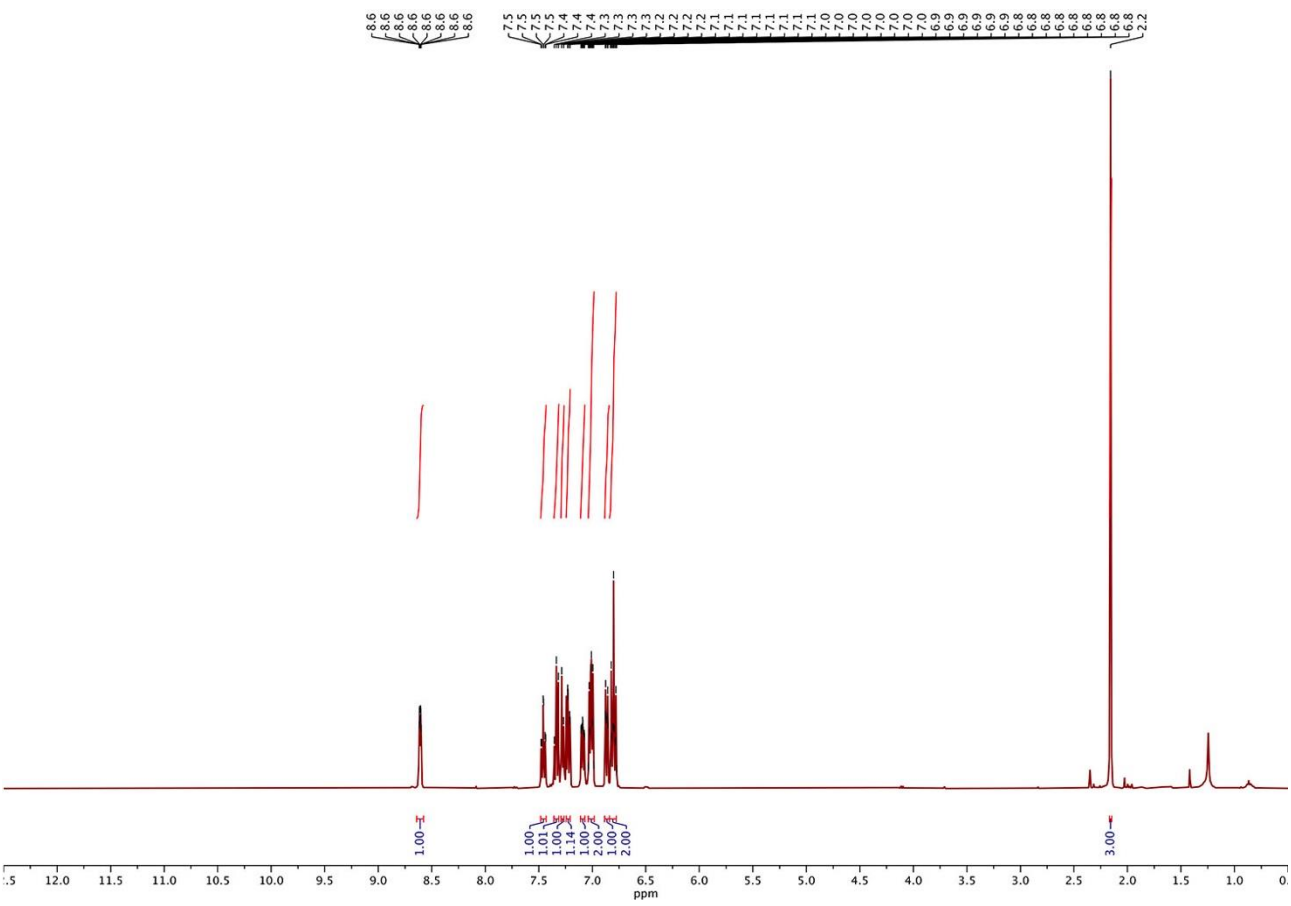

Figure S32. $^{13}C\{^{1}H\}$ NMR (101 MHz, $CDCl_3$) for **4e**

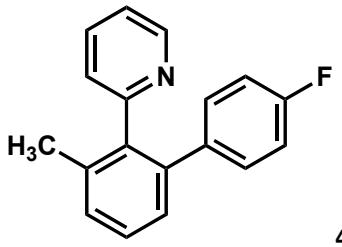

4e

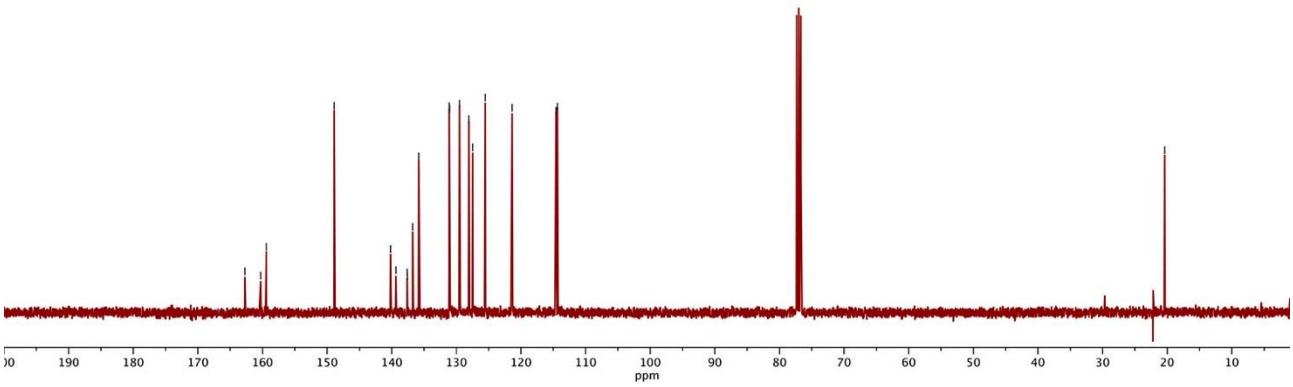

Figure S33. ^{19}F NMR (376.5 Hz, $CDCl_3$) for **4e**

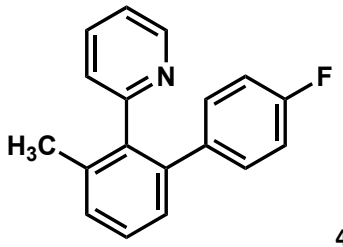

4e

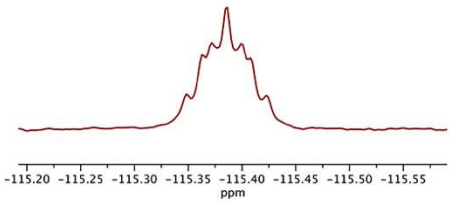

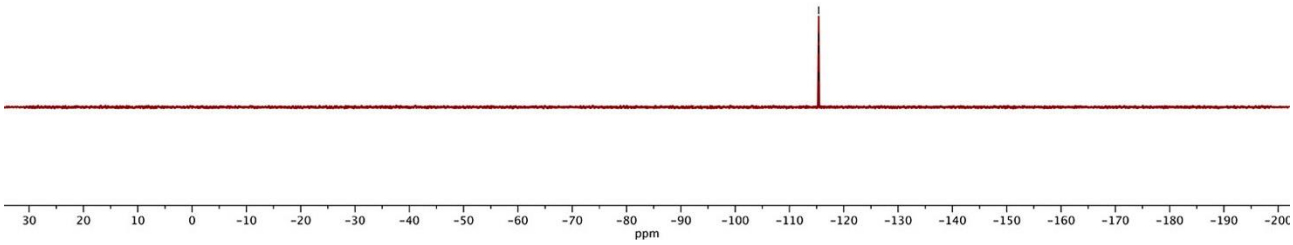

Figure S34. ^{1}H NMR (401 MHz, $CDCl_3$) for **4f**

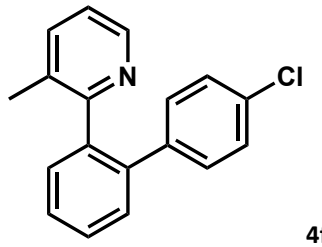

4f

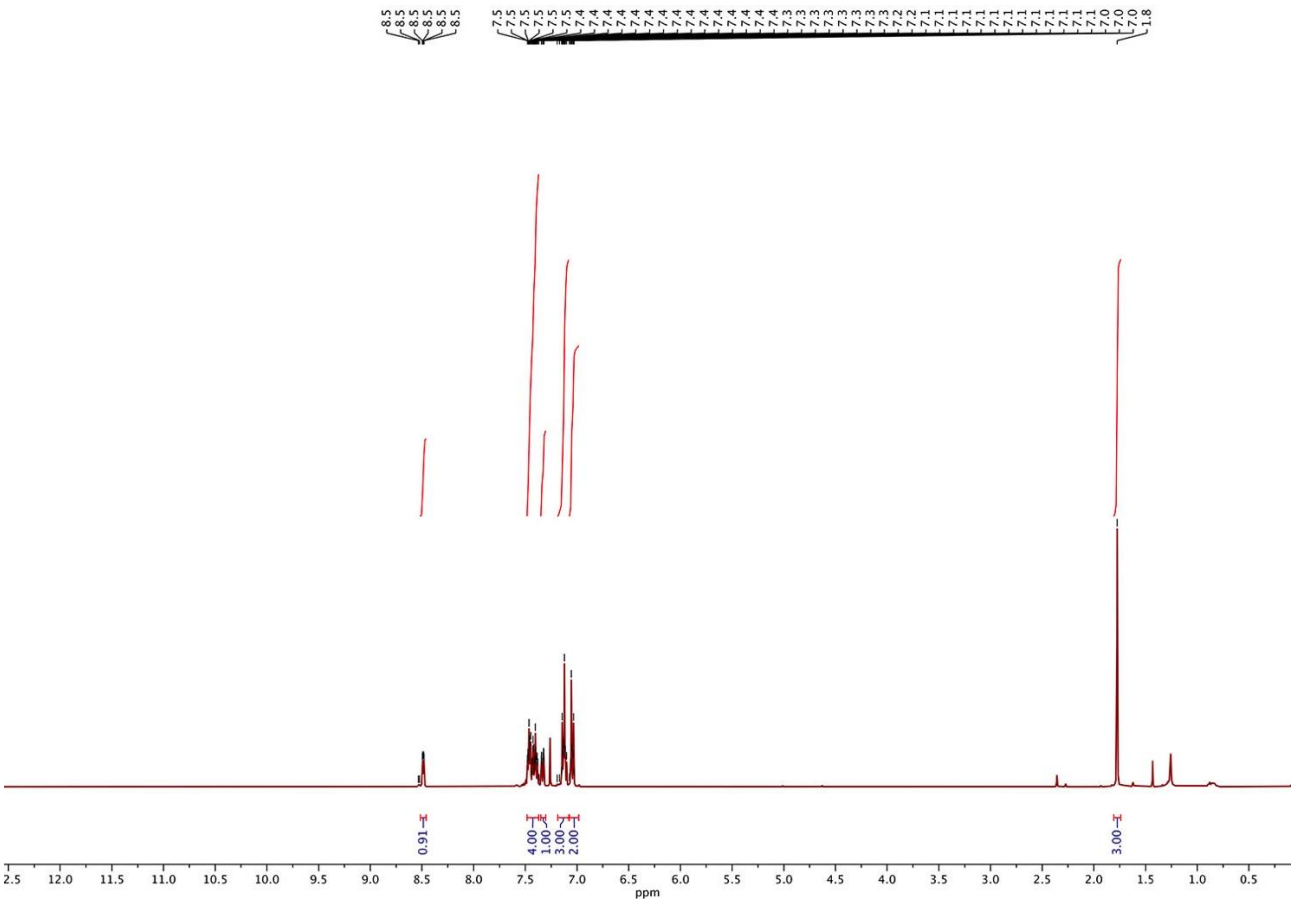

Figure S35. $^{13}C\{^{1}H\}$ NMR (101 MHz, $CDCl_3$) for **4f**

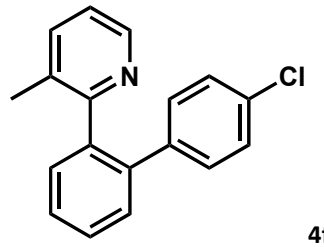

4f

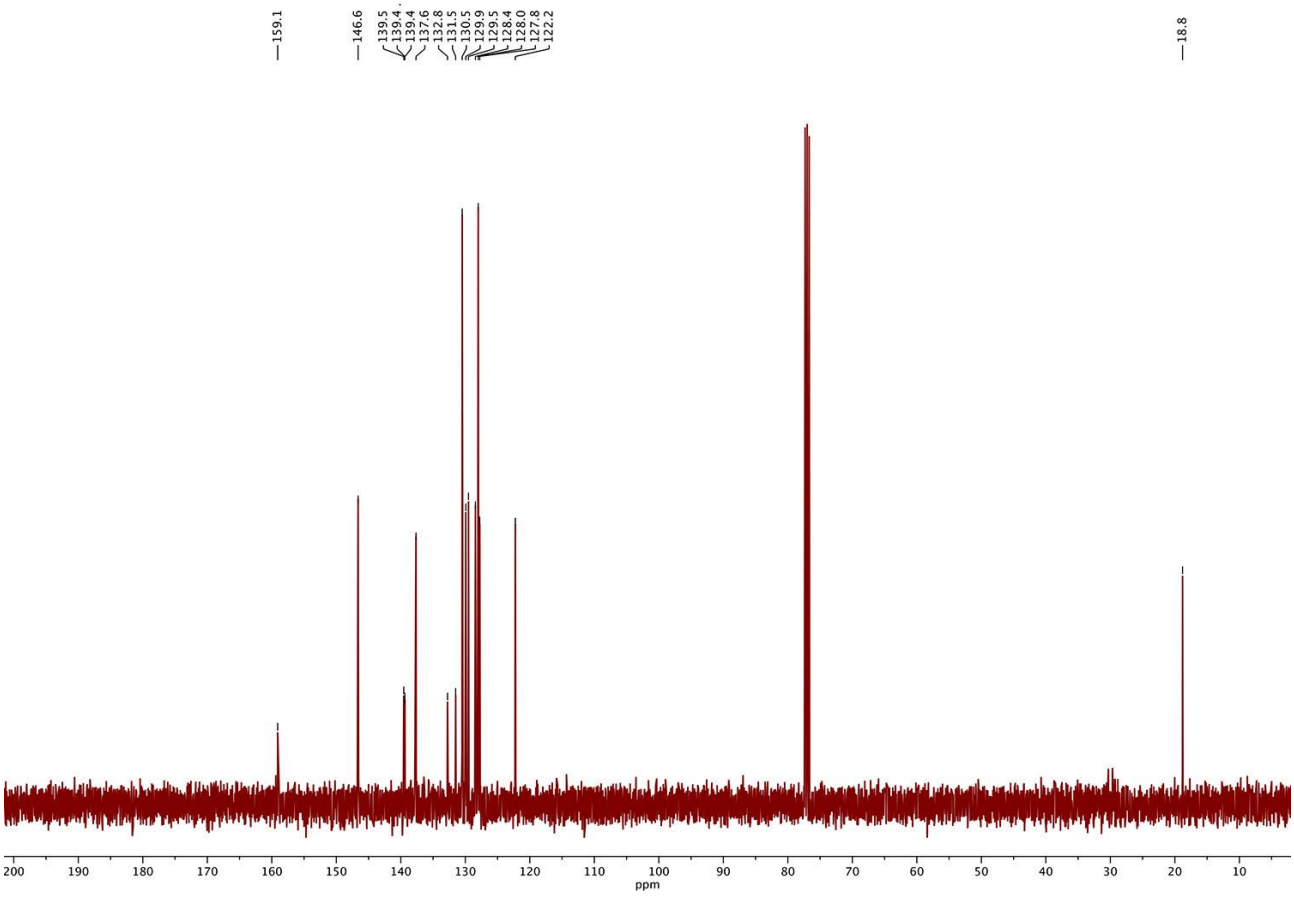

Figure S36. ^{1}H NMR (401 MHz, $CDCl_3$) for **4g**

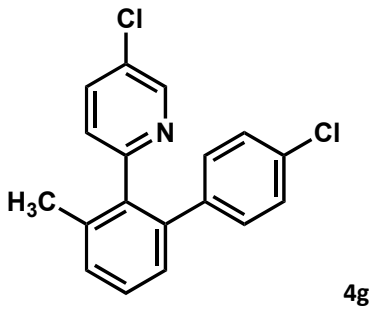

4g

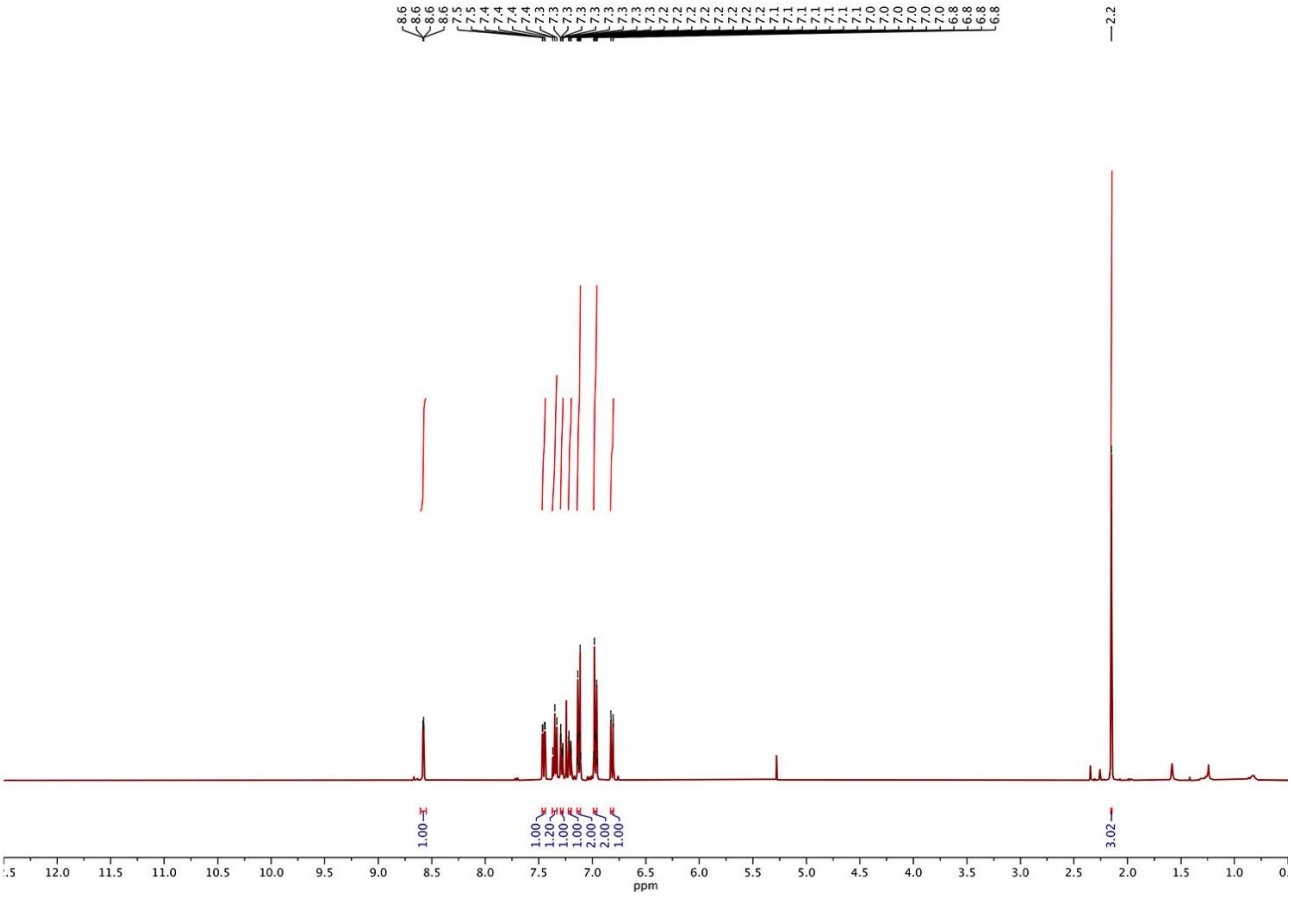

Figure S37. $^{13}C\{^{1}H\}$ NMR (101 MHz, $CDCl_3$) for **4g**

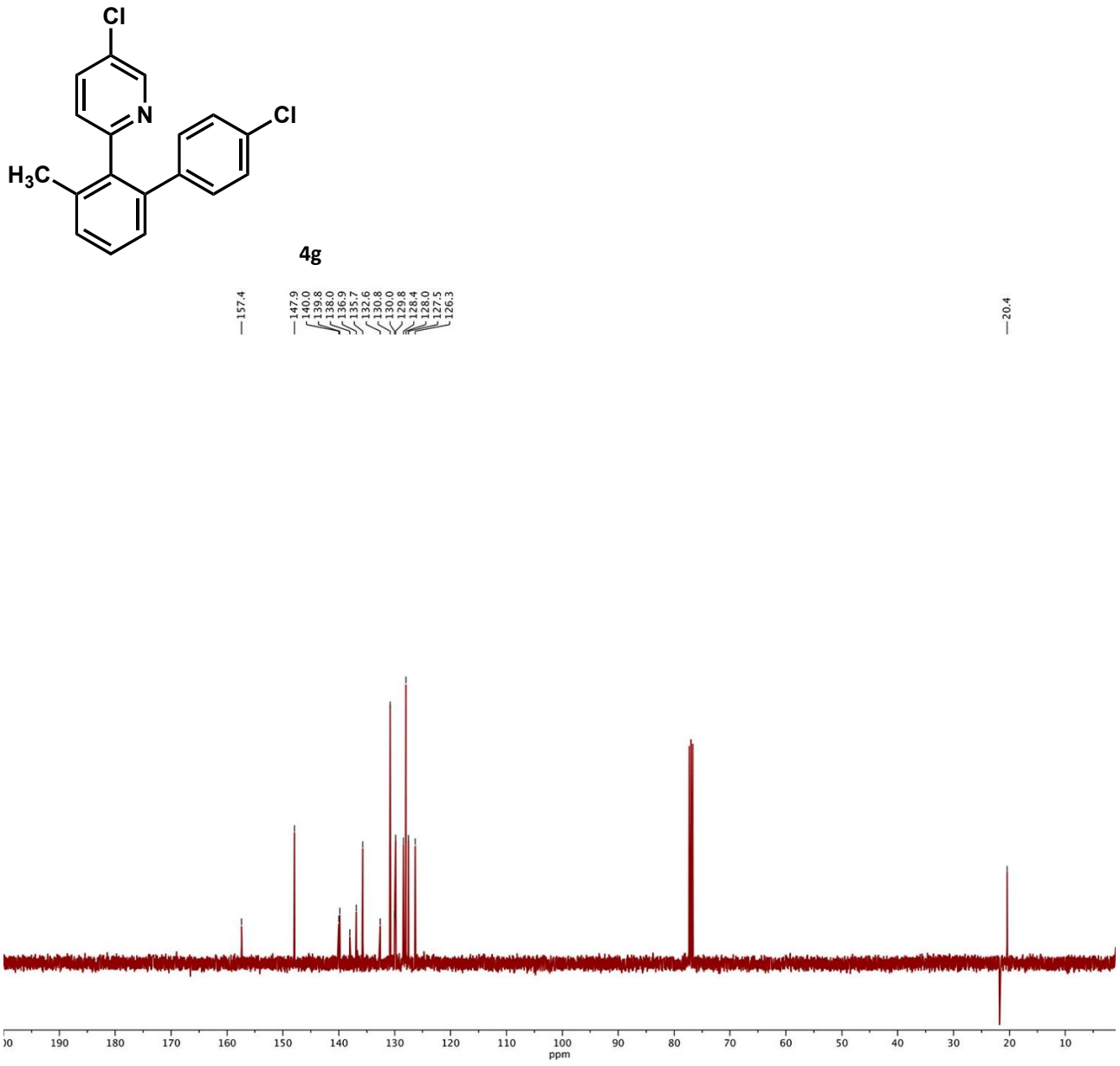

Figure S38. ^{1}H NMR (401 MHz, $CDCl_3$) for **4h**

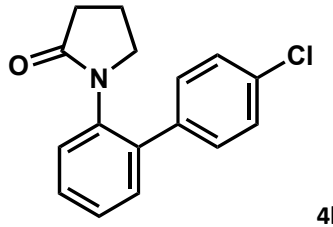

4h

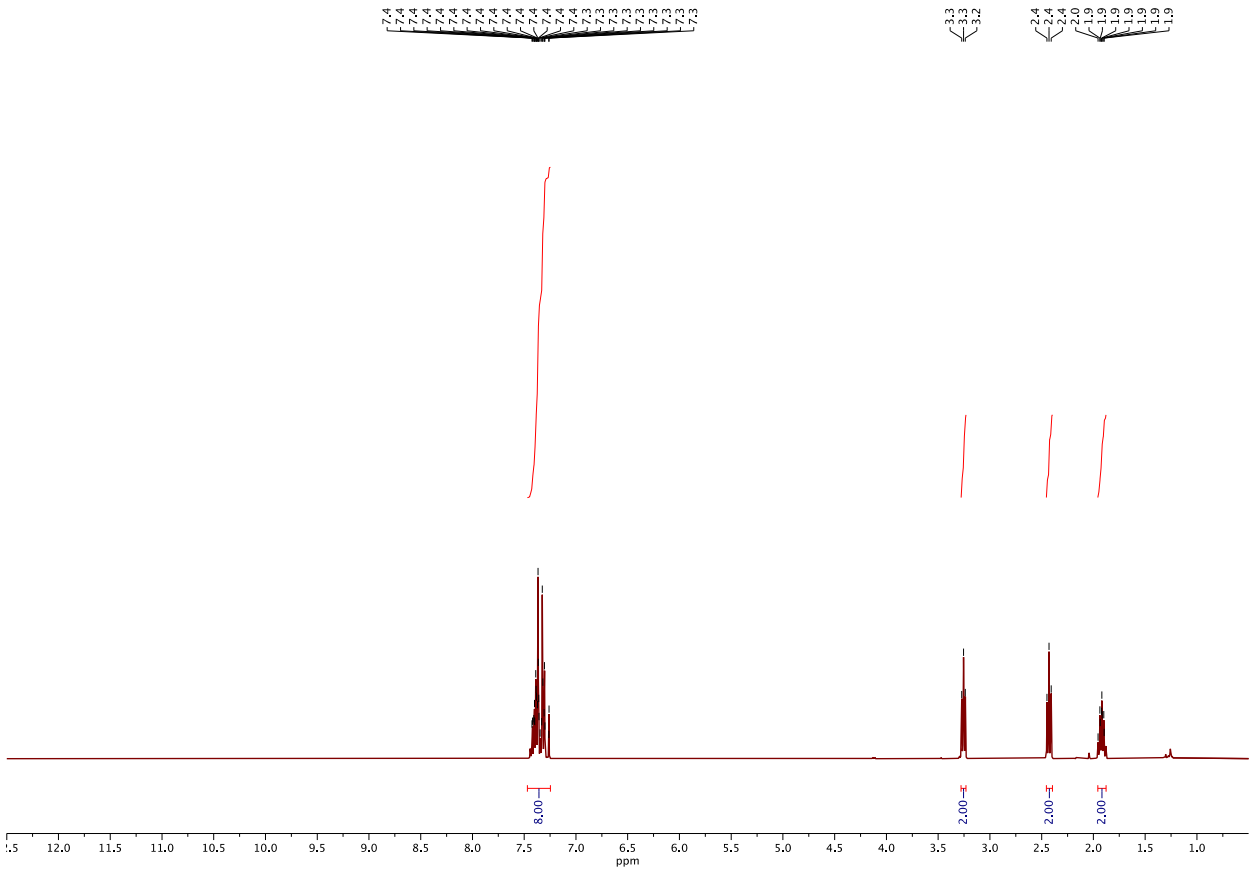

Figure S39. $^{13}C\{^{1}H\}$ NMR (101 MHz, $CDCl_3$) for **4h**

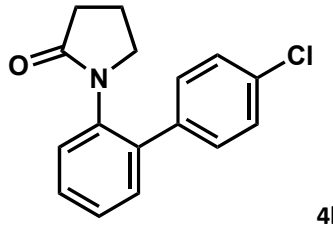

4h

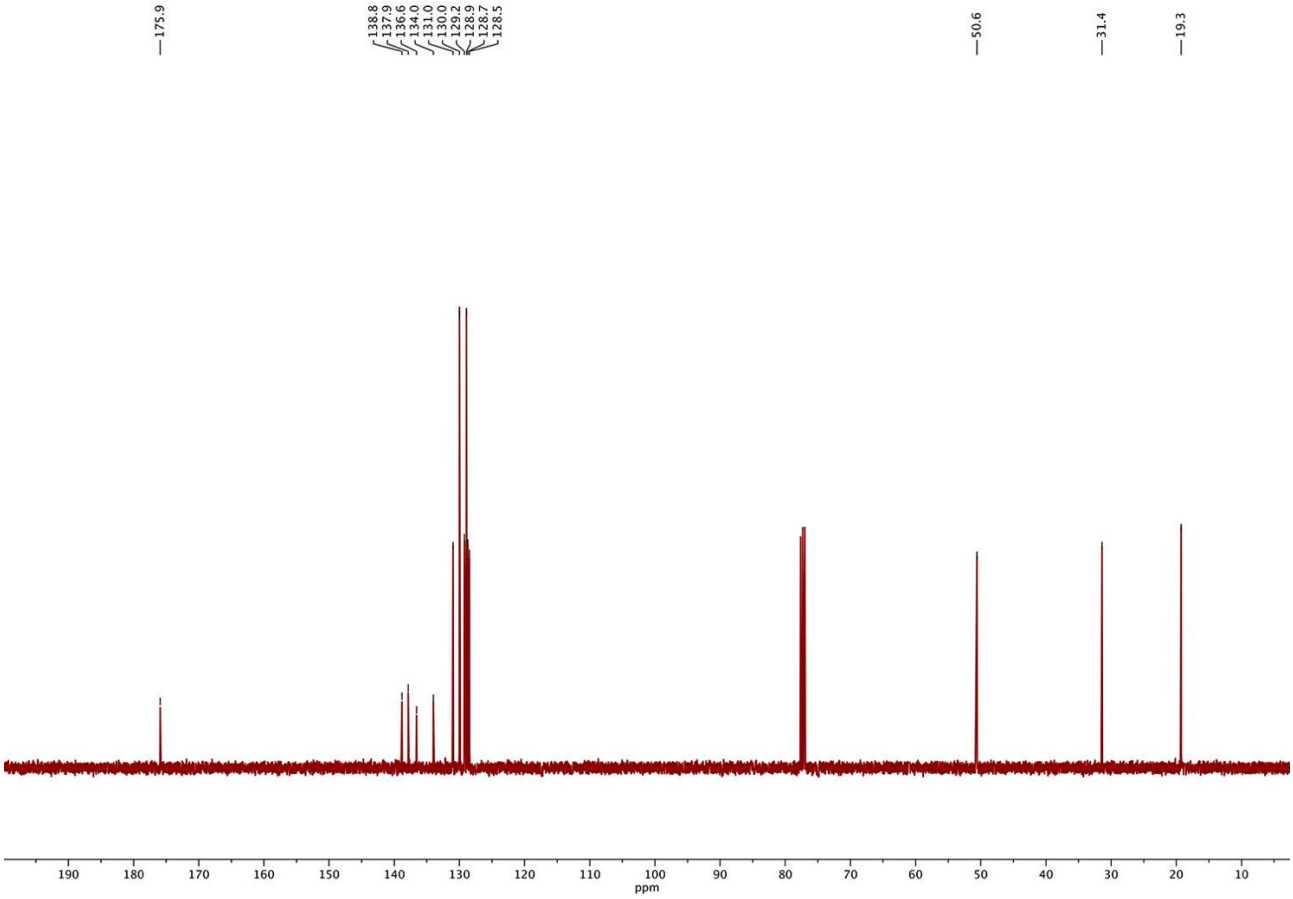

Figure S40. ^{1}H NMR (401 MHz, $CDCl_3$) for **4l**

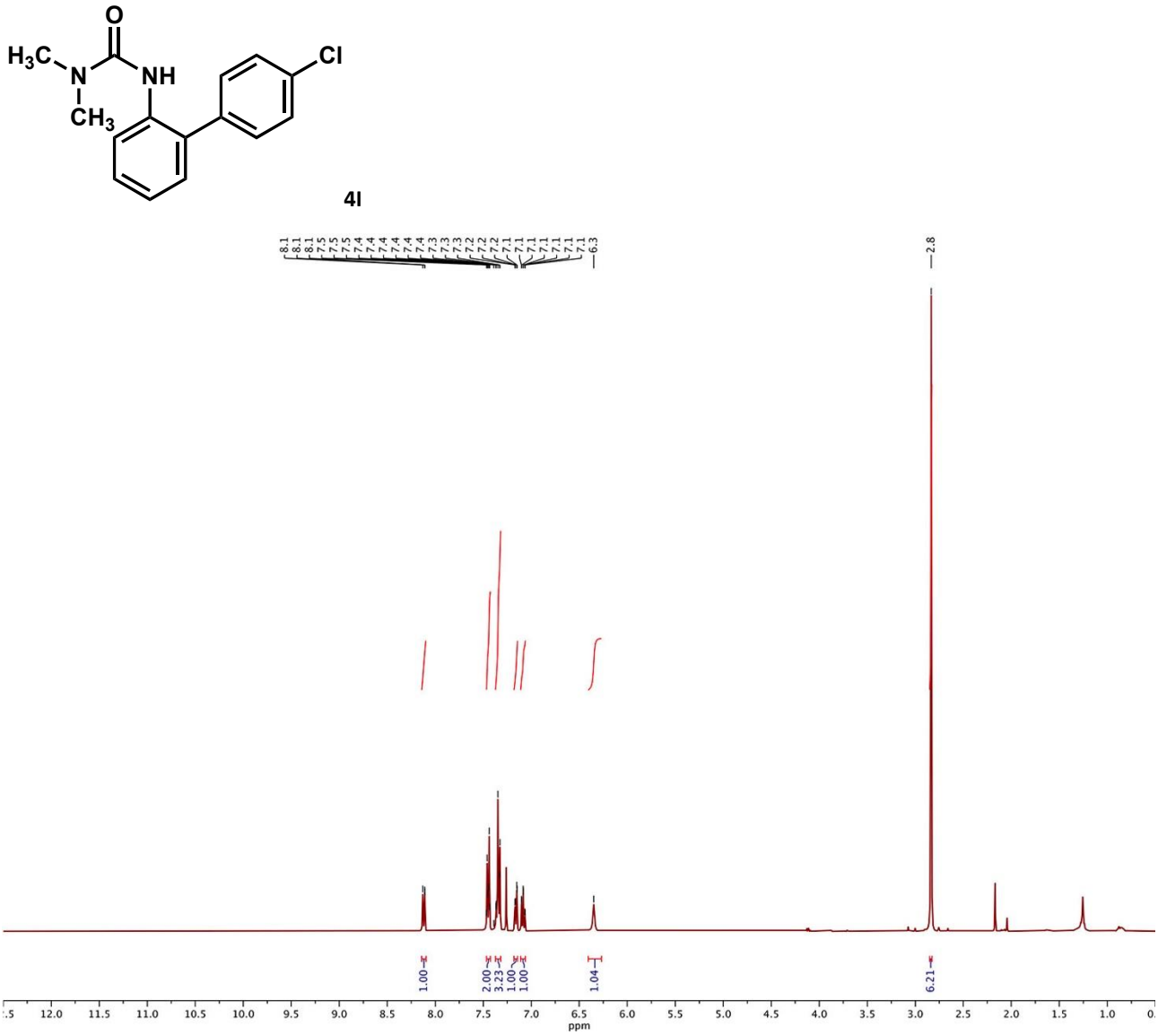

Figure S41. $^{13}C\{^{1}H\}$ NMR (101 MHz, $CDCl_3$) for **4l**

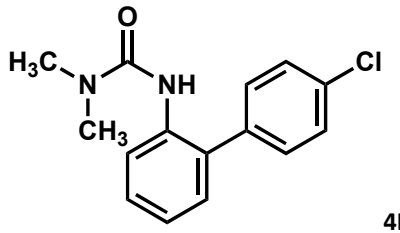

4l

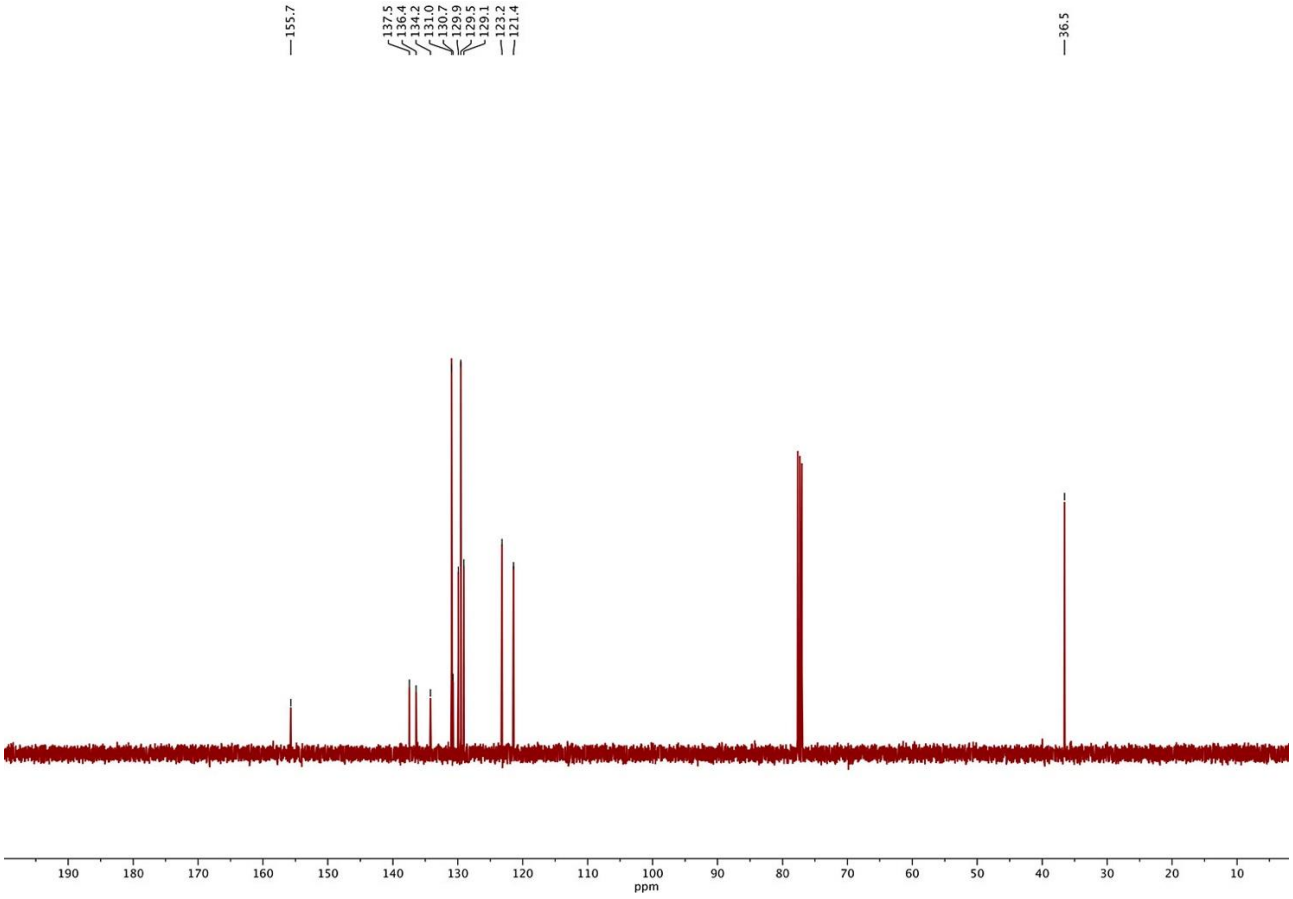

Figure S42. ^{1}H NMR (401 MHz, $CDCl_3$) for **4j**

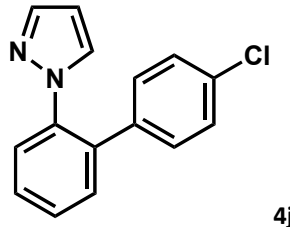

4j

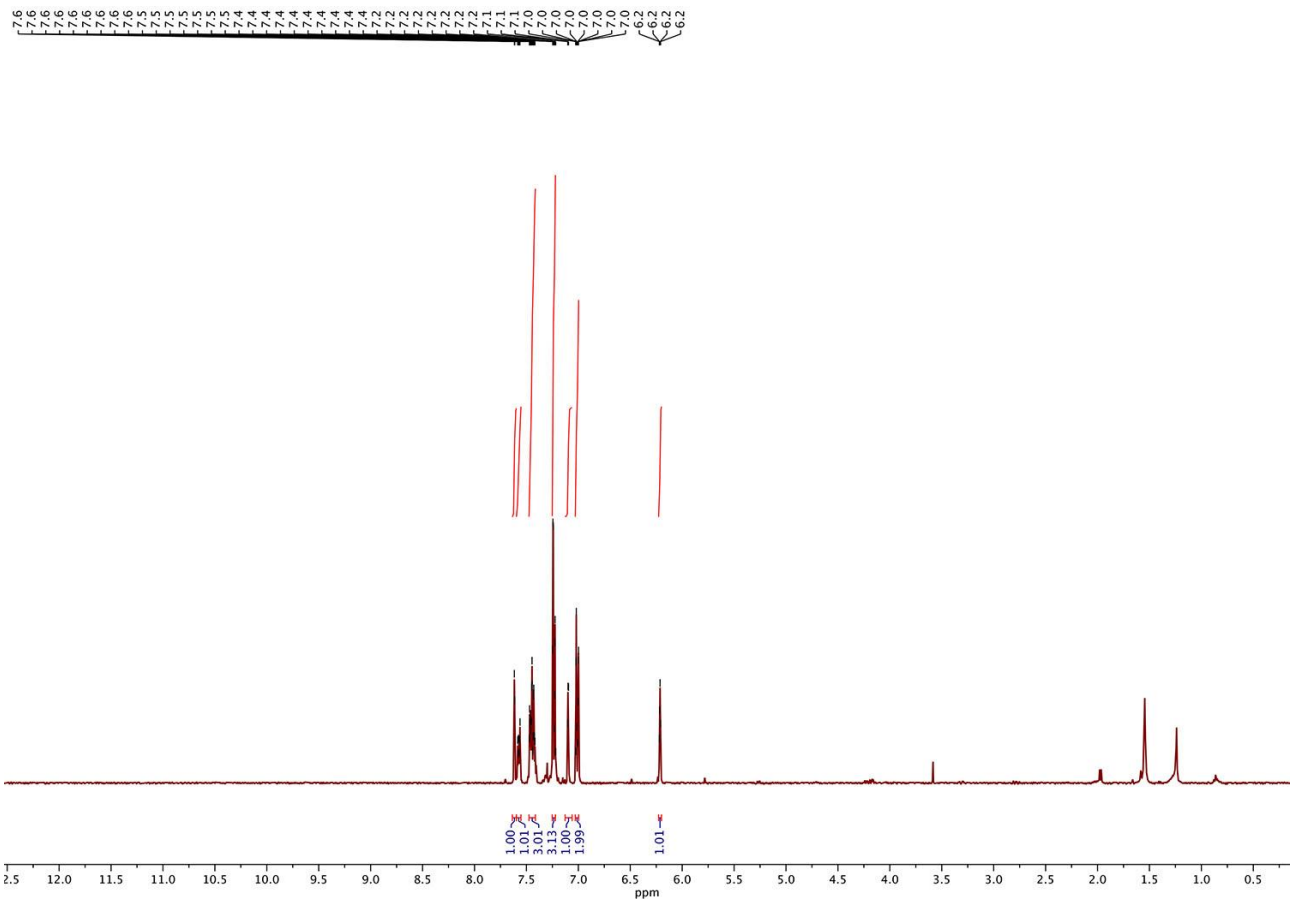

Figure S43. $^{13}C\{^{1}H\}$ NMR (101 MHz, $CDCl_3$) for **4j**

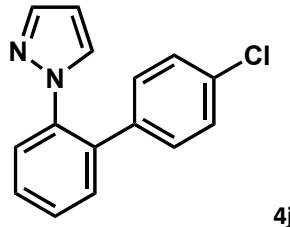

4j

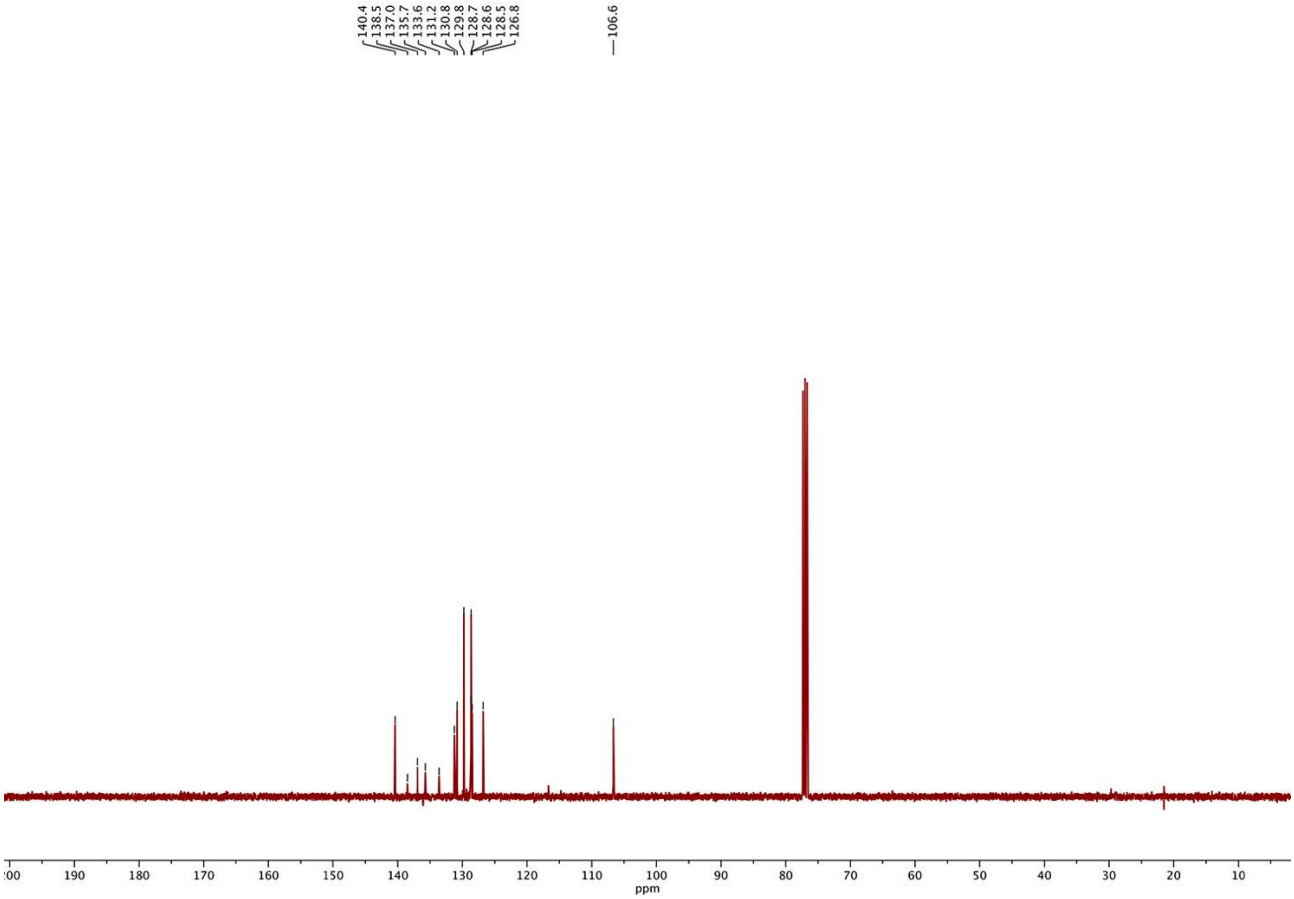

Figure S44. ^{1}H NMR (401 MHz, $CDCl_3$)for **4k**

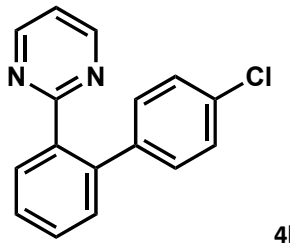

4k

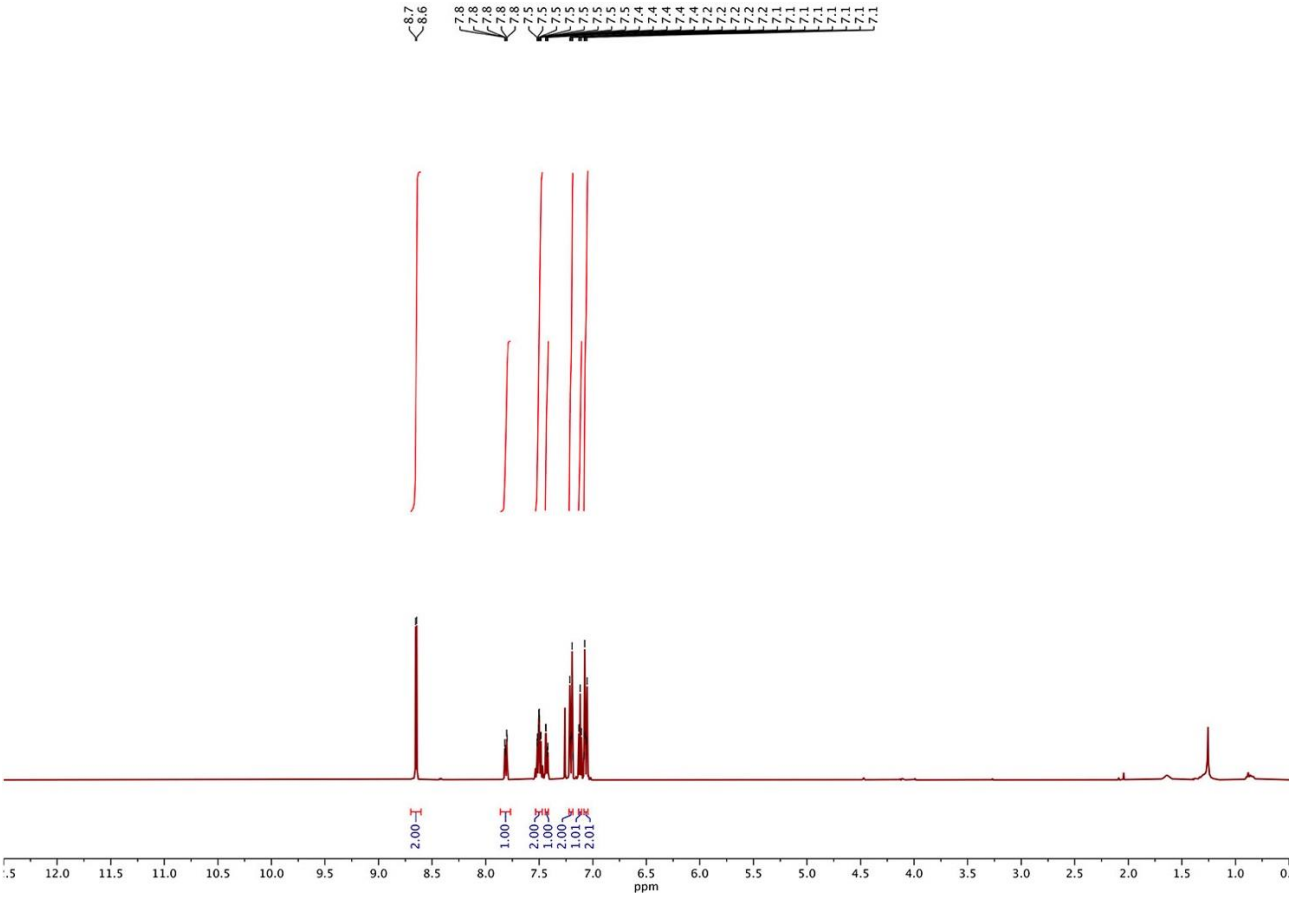

Figure S45. $^{13}C\{^{1}H\}$ NMR (101 MHz, $CDCl_3$) for **4k**

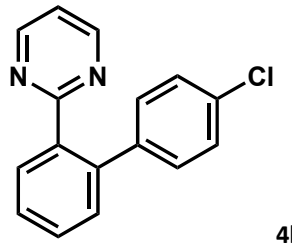

4k

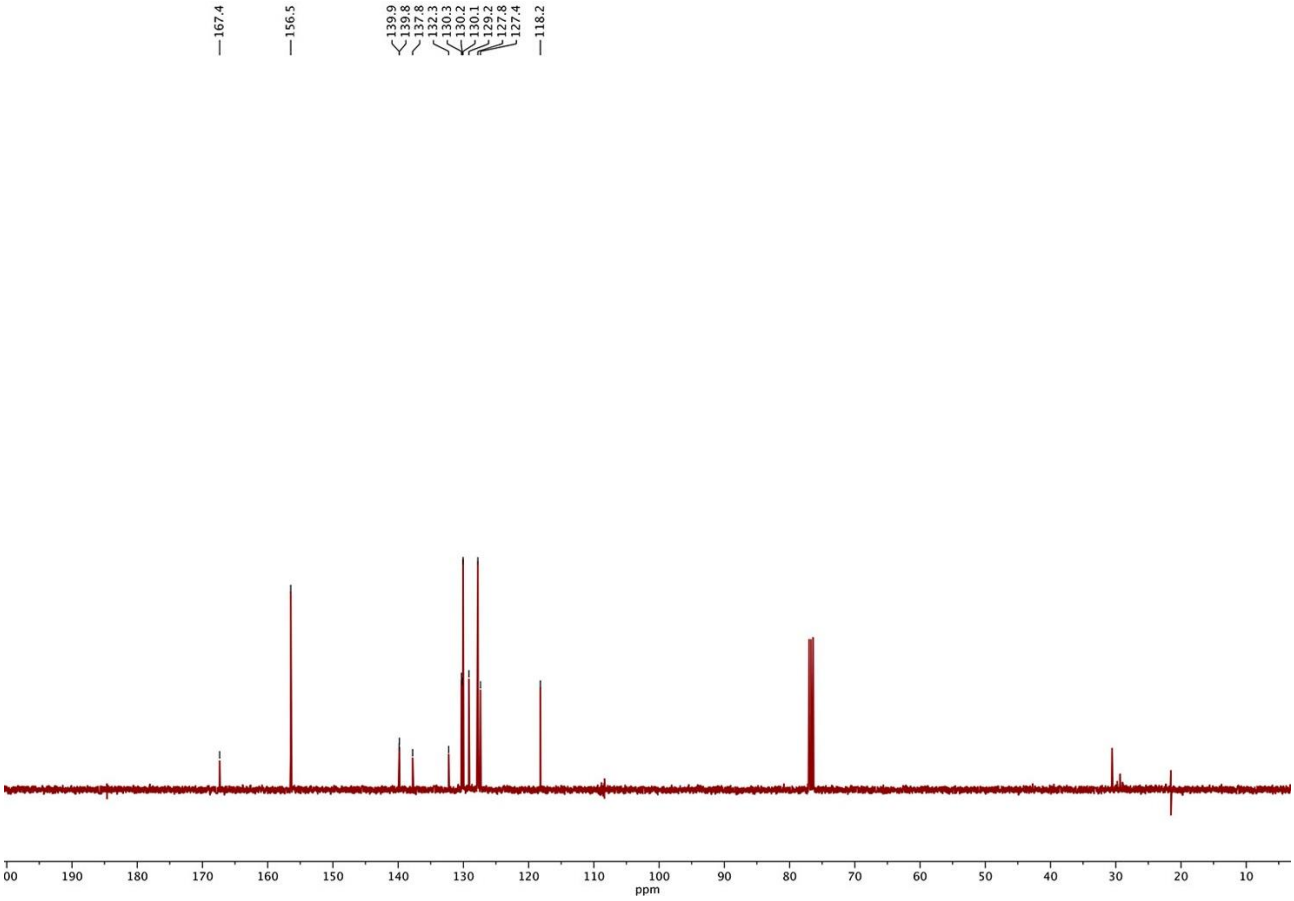

Figure S46. ^{1}H NMR (401 MHz, $CDCl_3$) for **4k'**

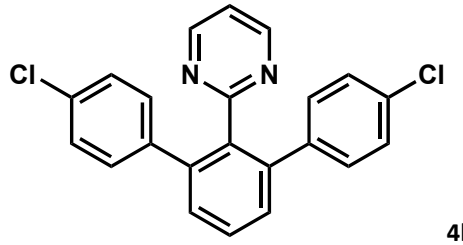

4k'

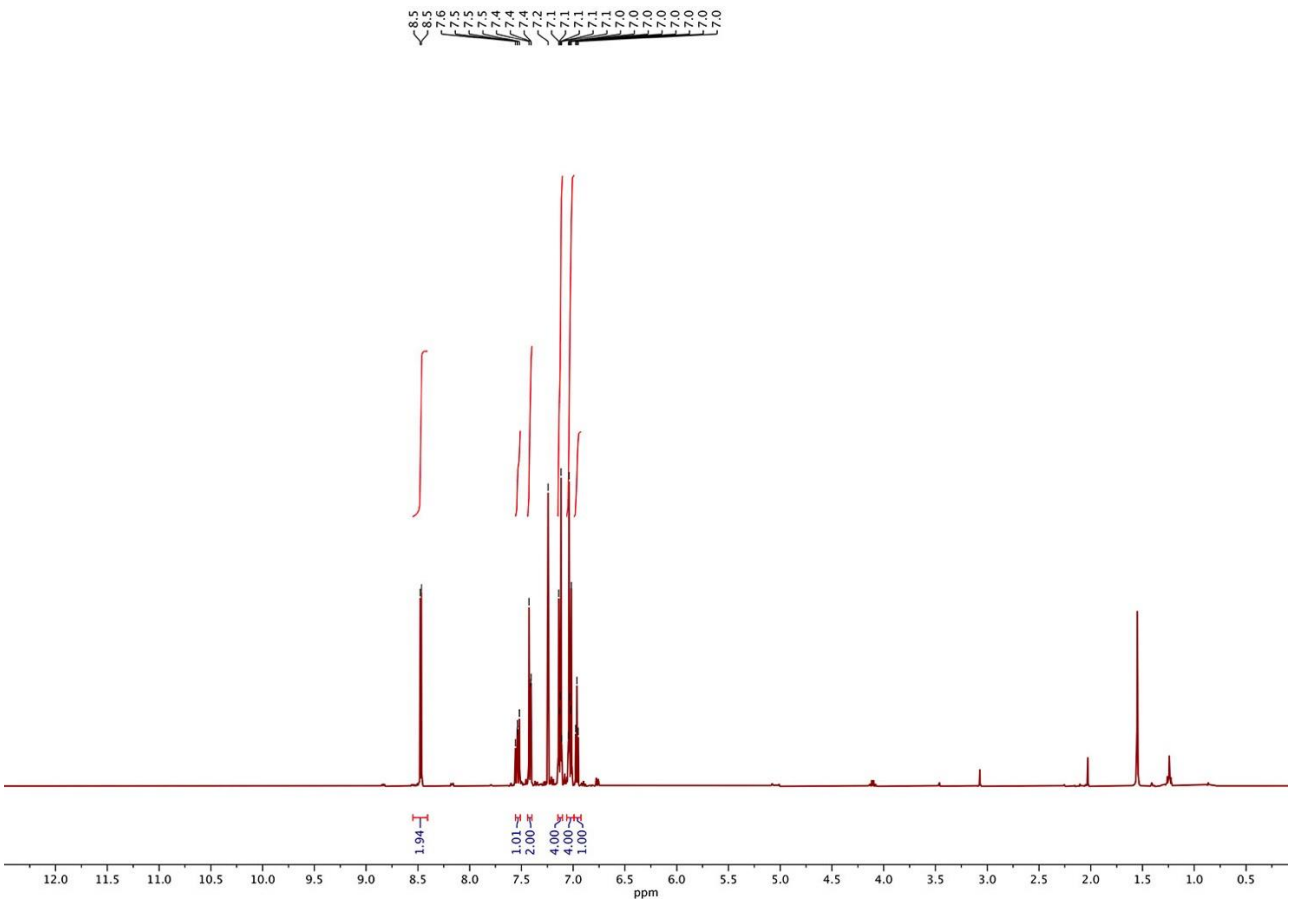

Figure S47. $^{13}C\{^{1}H\}$ NMR (101 MHz, $CDCl_3$) for **4k'**

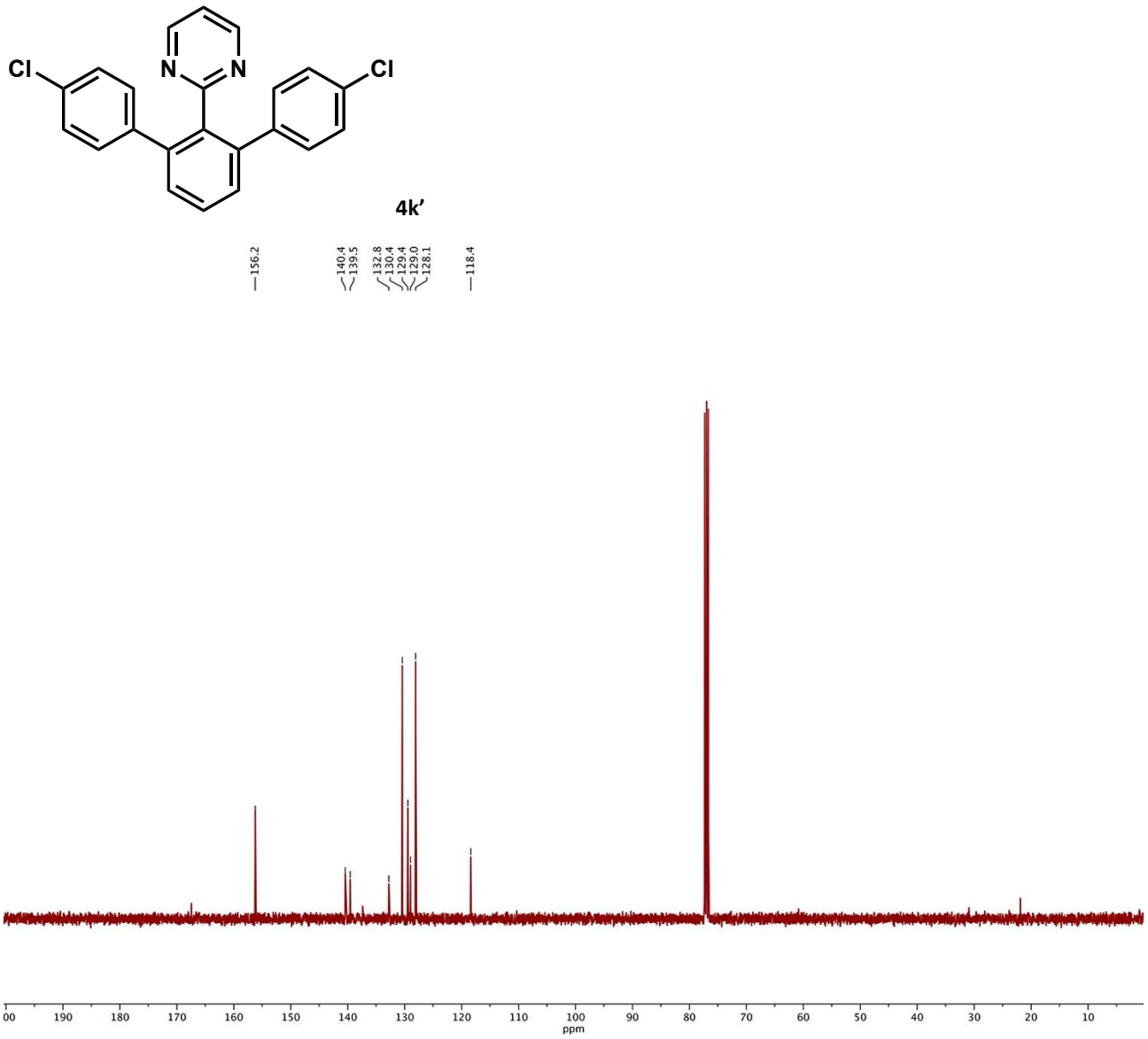

Figure S48. ^{1}H NMR (401 MHz, $CDCl_3$) for **4l**

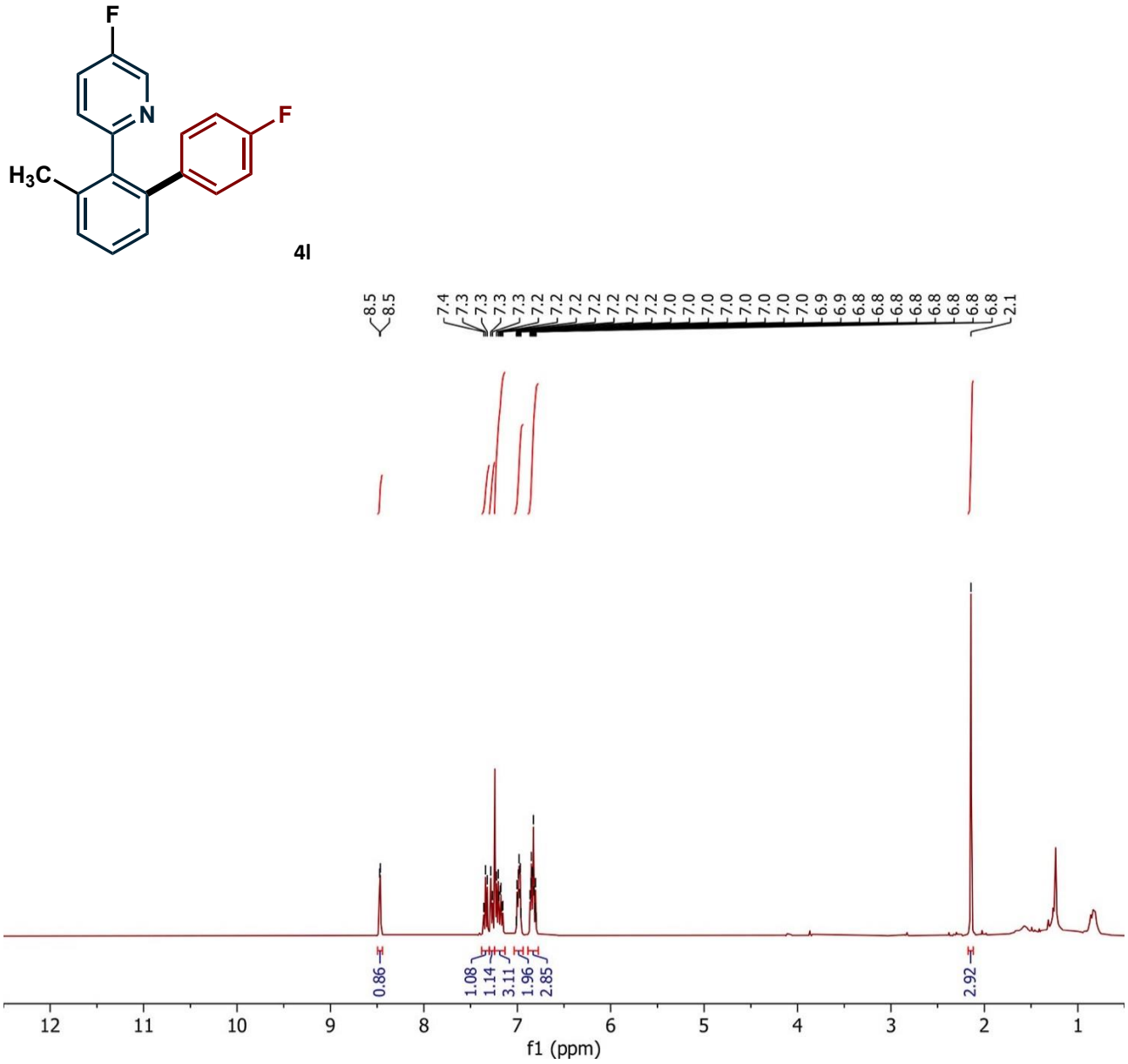

Figure S49. $^{13}C\{^{1}H\}$ NMR (101 MHz, $CDCl_3$) for **4l**

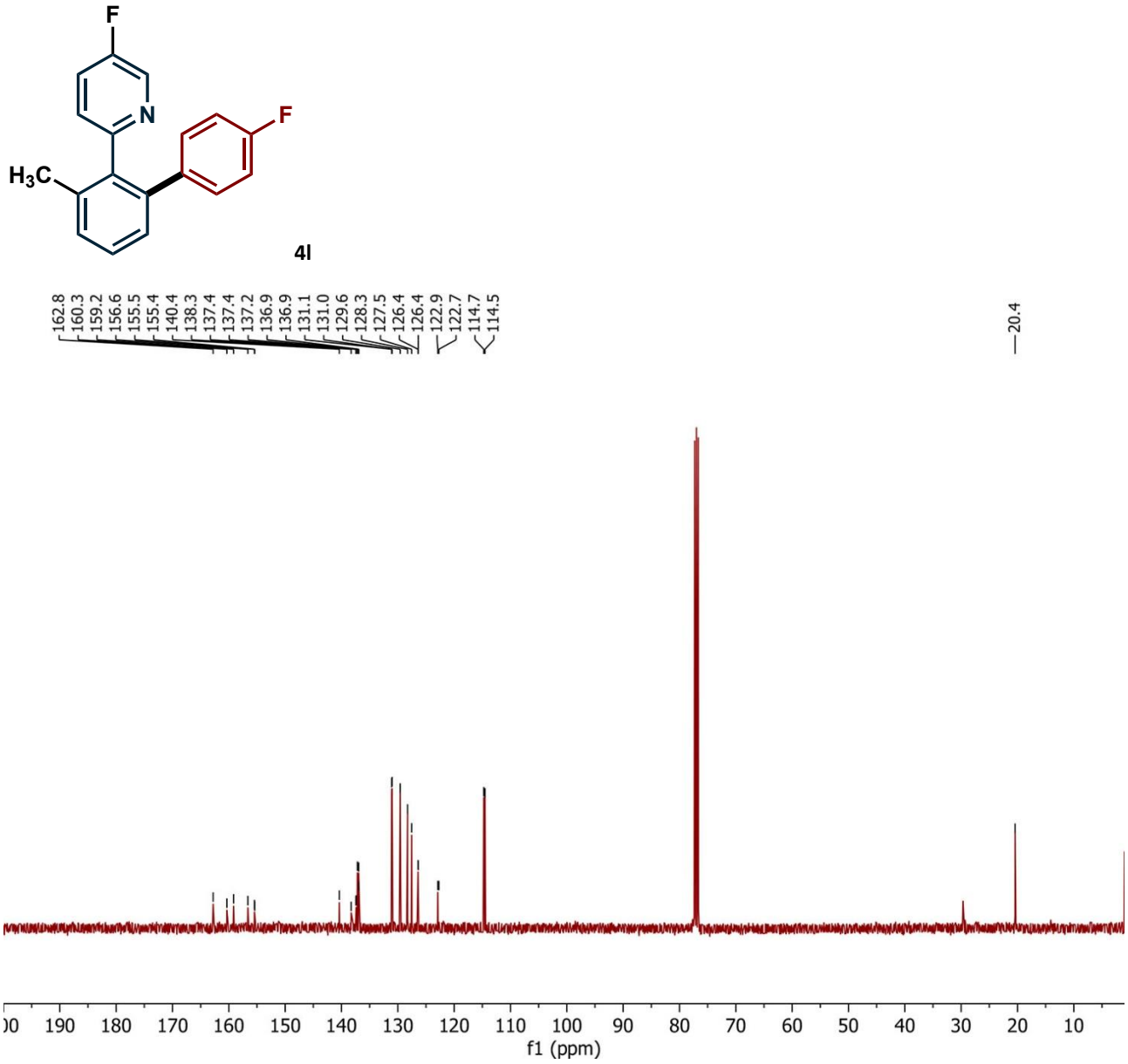

Figure S50. ^{19}F NMR (376.5 Hz, $CDCl_3$) for **4l**

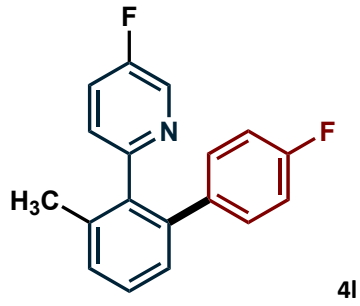

4l

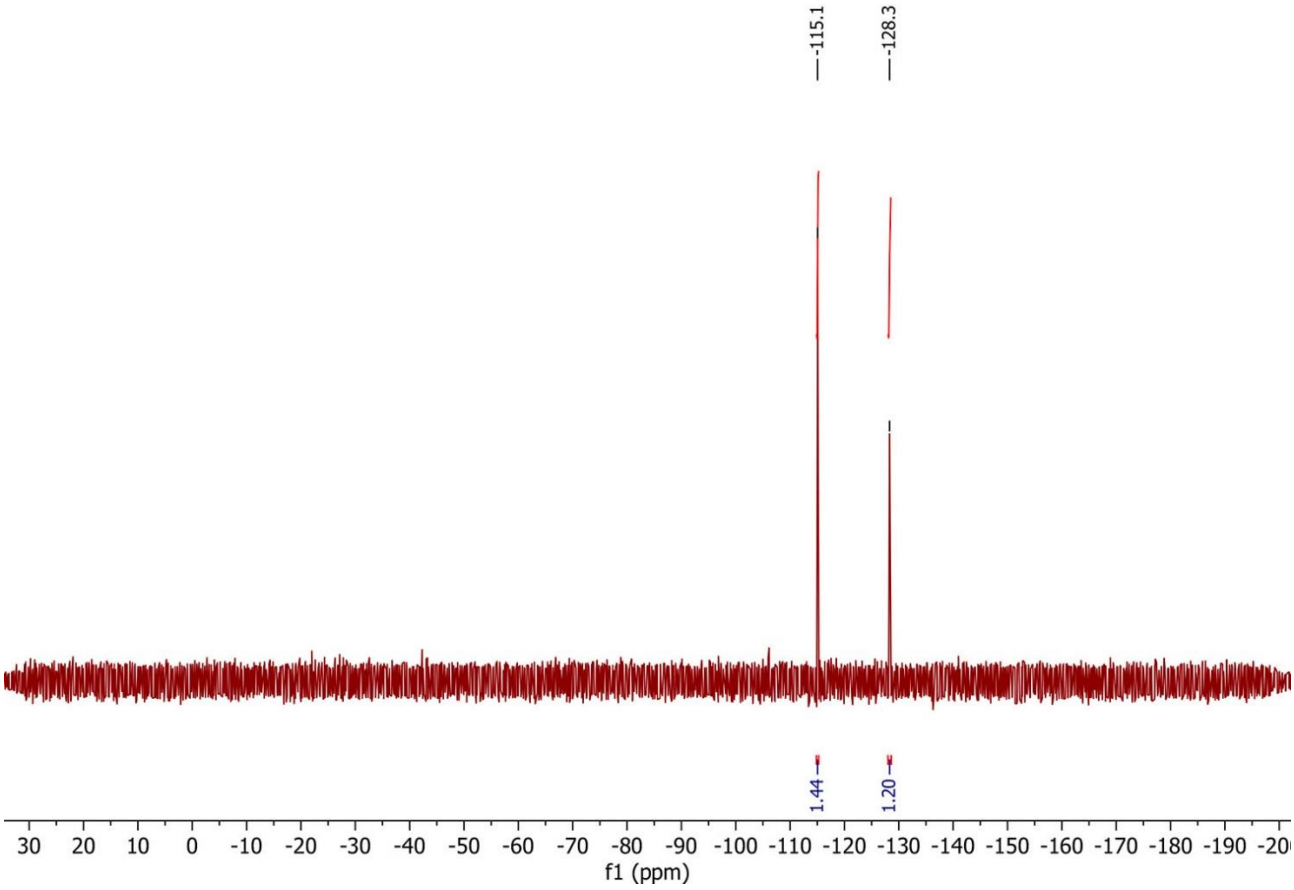

Figure S51. ^{1}H NMR (401 MHz, $CDCl_3$) for **4m**

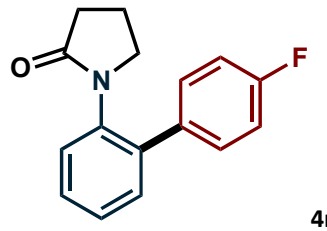

4m

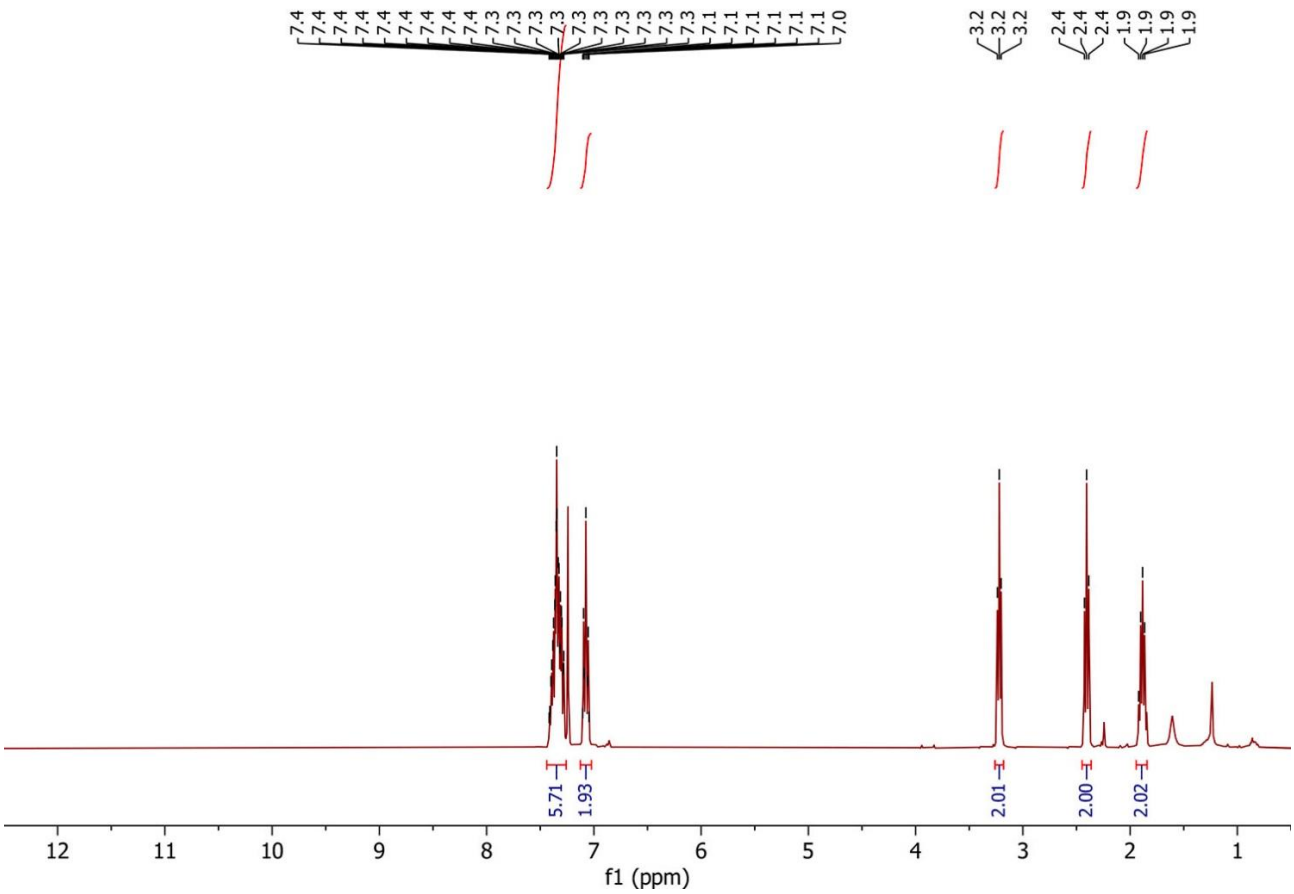

Figure S52. $^{13}C\{^{1}H\}$ NMR (101 MHz, $CDCl_3$) for **4m**

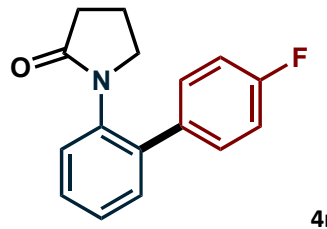

4m

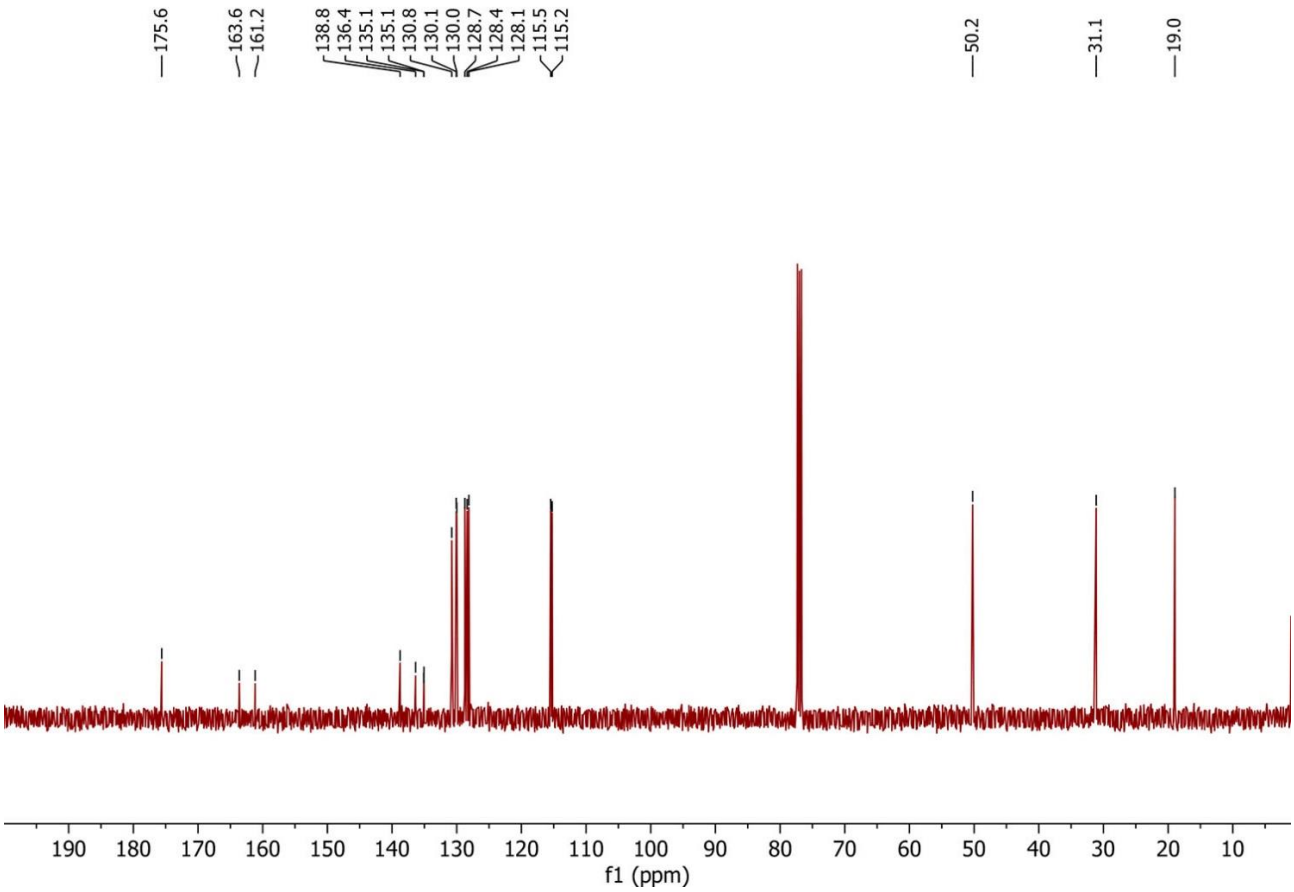

Figure S53. ^{119}F NMR (376.5 Hz, $CDCl_3$) for **4m**

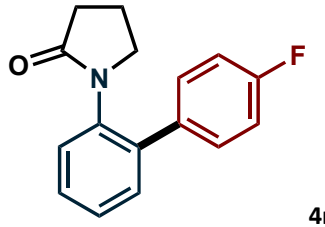

4m